ELECTRON PARAMAGNETIC RESONANCE OF Gd^{3+} IN $SmCl_3.6H_2O$, $NdCl_3.6H_2O$ AND $YCl_3.6H_2O$

Michael Skarpathiotakis

A THESIS

in

The Department

of

Physics

Presented in Partial Fulfillment of the Requirements
for the Degree of Master of Science at
Sir George Williams University
Montreal, Canada

April, 1974

Michael Skarpathiotakis

Electron Paramagnetic Resonance of Gd^{3+} in $SmCl_3 \cdot 6H_2O$, $NdCl_3 \cdot 6H_2O$ and $YCl_3 \cdot 6H_2O$

ABSTRACT

The paramagnetic resonance of dilute Gd^{3+} impurities in single crystals of $SmCl_3.6H_2O$, $NdCl_3.6H_2O$ and $YCl_3.6H_2O$, grown in this laboratory, was studied at room temperature. A six line spectrum for H||Z and a seven line spectrum for H||X, both corresponding to $\Delta M=\pm 1$, were observed in the case of Gd^{3+} in $SmCl_3.6H_2O$ and $NdCl_3.6H_2O$. In the case of Gd^{3+} in $YCl_3.6H_2O$ a seven line spectra both for H||Z and H||X corresponding to $\Delta M=1$ was observed.

The variation of the spectrum for H at various angles in the ZX-plane was analyzed, and the experimental parameters were calculated for the spin-Hamiltonian of the system. The analysis was carried out by diagonalizing the full spin-Hamiltonian, rather than by the use of perturbation theory methods as done by previous researchers. All the spin-Hamiltonian parameters were calculated individually in contrast to the perturbation theory approach which does not enable one to individually calculate the parameters, allowing calculation of only some of their linear combinations.

One purpose of the experiment was to check the isotropy of the g-factor of Gd^{3+} in $SmCl_3.6H_2O$ as observed by Singh et al[10]. A definite anisotropy was observed by us which is consistent with similar Gd^{3+} rare earth crystals.

The probable admixture of the next-higher electronic state $^6P_{7/2}$ with the ground state $^8S_{7/2}$ was also estimated.

TABLE OF CONTENTS

LIST OF FIGURES

LIST OF TABLES

ACKNOWLEDGEMENTS

The author wishes to thank Professor S. K. Misra for suggesting the thesis problem and for his constant supervision, encouragement and advice during the course of the research, He is also grateful to Professor B. Frank for many useful discussions. Assistance in the performance of the experiment from his fellow graduate student G.R. Sharp and suggestions from Dr. Y. H. Shing of McGill University re computer analysis of the data, and expert typing of the thesis by Miss E. Henley are also acknowledged.

This work was partially supported by Professor Misra's N.R.C. grant.

CHAPTER I

INTRODUCTION

When a paramagnetic substance is placed in a steady magnetic field Zeeman splitting of the energy levels occurs, and photons having energies equal to the gaps between the Zeeman levels may induce transitions. The energy absorbed as a function of magnetic field strength is referred to as the paramagnetic resonance spectrum of the substance.[1] There are several classes of substances which are paramagnetic due to the resultant total angular momentum possessed by the electrons.

One such class is the rare-earth group of elements the ions of which possess partly-filled inner electronic shells. Substances having these ions incorporated in them are also referred to as being paramagnetic.

The interpretation of the results on paramagnetic resonance is simpler if single crystals are used. Paramagnetic resonance then gives direct and accurate information on the lowest energy level which results from the splitting of the ion's ground state.

The lattice crystalline environment affects the ground state of the ion in a complex way, so that the Zeeman spectrum of ions in a solid usually differs markedly from that of a free ion.

The spin-Hamiltonian method provides a very concise description of how energy levels depend on the magnetic field, orientation and other system parameters, thereby making it possible to describe the resonance properties of an ion in terms of a relatively small number of constants.

When Zeeman transitions are induced in the system of paramagnetic ions by means of a radio-frequency magnetic field, there is a net absorption of energy from the r.f. field. This occurs because the induced transition probabilities are large compared with the probability of spontaneous emission. The initial populations of the levels obey the Boltzmann distribution law so that the lower of two levels is always more densely populated than the upper one.

In the rare-earth group, the magnetic electrons are in the 4f shell. The free-ion spectra indicate that the configurations split into terms which are characterized by a definite L and S. The spin and orbital angular momentum vectors are coupled by the spin-orbit interaction; the total angular momentum J remains a good quantum number.

The Gd^{3+} $4f^7$ configuration gives rise to an $^8S_{7/2}$ free-ion ground state, according to Hund's rules. From experiments it is known that this ground state is not enough to explain the EPR spectra of Gd^{3+} in a solid, since the g-value of the ground state is less than the expected free-electron value.

The basic technique used for studying resonance depends on observing the damping of a resonant circuit due to the energy absorbed in the sample from the r.f. field. If the resonant circuit is in one arm of an a.c. bridge the absorption produces an imbalance in the bridge.

The spectrometer employs a fixed radio frequency, while the d.c. magnetic field is variable from a few gauss to several kilogauss.

CHAPTER II

THEORY

1. HISTORICAL SURVEY

Electron Paramagnetic Resonance was discovered in 1945 by Zavoisky[2], using newly-developed microwave techniques to study the Zeeman levels in paramagnetic substances.

Soon afterwards experiments were reported by Cummerow and Halliday, and by Bleaney and Penrose. The main progress in the techniques of measurement since then has come from the Oxford group of Bleaney and Griffith and their co-workers. The theoretical apparatus for the interpretation of these results was developed by Pryce and his co-workers Abragam, Stevens, Elliott and Judd.

The study of the paramagnetic properties of the Gadolinium ion Gd^{3+} has a long and interesting history.[3] It was natural, when the technique of electron paramagnetic resonance was developed, that the Gd^{3+} compounds, having s-states as ground states, would be studied extensively. Interest in the paramagnetic properties of this ion was renewed in 1956, after its successful utilization by Scovil et al.[4a] as the active material in the first operational solid state maser. Many scientists have worked with the theoretical or experimental aspects of Gd^{3+} doped in different hosts, and at present it is a very active field of research. (The book "Paramagnetic Resonance" by W. Low[1] furnishes an excellent bibliography which has been used extensively in the above historical survey.)

2. GENERAL HAMILTONIAN OF THE "FREE ION"

The lowest and excited energy levels of an ion situated in a crystal of given symmetry are modified by the crystalline surroundings.[1]

The most important interaction in an ion is given by the Coulomb term. This consists of the interaction of the electrons with the nuclear charge Ze and the mutual repulsion of the electrons. In the non-relativistic approximation, together with the electronic kinetic energy, it is given by

$$V_c = \sum_{k=1}^{N} (\vec{p}_k^2/2m - Ze^2/r_k) + \sum_{k>j=1}^{N} e^2/r_{kj}$$

$\vec{p}_k$ is the linear momentum of electron k. (k,j label the electrons in the ion); $\vec{r}_k$ is the radius vector extending from the nucleus to the k^{th} electron ($r_k = |\vec{r}_k|$); the whole expression is summed over all N electrons in the ion. This Coulomb repulsion is different for different states of the same configuration and correspondingly leads to various energy levels or "term values". The next most important interaction is a magnetic interaction V_{LS} between the electron spin $\vec{s}_k$ and the orbital momentum $\vec{l}_k$. It is given by $V_{LS} = \sum_{j,k} a_{jk} \vec{l}_j \cdot \vec{s}_k + b_{jk} \vec{l}_j \cdot \vec{l}_k + c_{jk} \vec{s}_j \cdot \vec{s}_k$ where a_{jk}, b_{jk}, c_{jk} are certain constants. If we consider states of definite L and S of the same configuration, i.e. Russell-Saunders coupling, the spin-orbit interaction can be written $\lambda \vec{L} \cdot \vec{S}$ where λ is known as the spin-orbit coupling constant for the ion. The much weaker spin-spin interaction V_{SS}, that is, the mutual interaction between the magnetic dipoles is expressed as follows: (β is the Bohr magneton)

$$V_{SS}=\sum_{j>k}\left\{\frac{\vec{s}_j.\vec{s}_k}{r_{jk}^3}-\frac{3(\vec{r}_{jk}.\vec{s}_j)(\vec{r}_{jk}.\vec{s}_k)}{r_{jk}^5}\right\}4\beta^2$$

These are the dominant terms of the free ion. If the nucleus has a spin I and quadrupole moment Q, the various terms are further split by two additional interactions V_N and V_Q where

$$V_N=2\gamma\beta\beta_N\left[\sum_k\left\{\frac{(\vec{l}_k-\vec{s}_k).\vec{I}}{r_k^3}+\frac{3(\vec{r}_k.\vec{s}_k)(\vec{r}_k.\vec{I})}{r_k^5}\right\}+\frac{8\pi\delta(\vec{r}_k)}{3}(\vec{s}_k.\vec{I})\right]$$

$$V_Q=\frac{e^2Q}{2I(2I-1)}\left[\sum_k\frac{I(I+1)}{r_k^3}-\frac{3(\vec{r}_k.\vec{I})^2}{r_k^5}\right]$$

Here β_N and γ refer to the nuclear magneton and nuclear gyromagnetic ratio, $\delta(\vec{r}_k)$ is the Dirac delta-function. The interaction with the external magnetic field H is given by $V_H=\sum_k\beta(\vec{l}_k+2\vec{s}_k).\vec{H}$ The direct interaction of the nucleus with the external field H is $V_h=-\gamma\beta_N\vec{H}.\vec{I}$ The general Hamiltonian of the free ion is given by the sum of all the above terms and is

$$\mathcal{H}=V_F+V_{LS}+V_{SS}+V_N+V_Q+V_H+V_h \qquad \ldots\ldots(2.1)$$

The order of magnitude of these interactions can be best estimated from observed atomic spectra for the rare earths: $V_F\sim 10^5 cm^{-1}$, $V_{LS}\sim 10^3 cm^{-1}$, $V_{SS}\sim$ cm^{-1}, $V_N\sim 10^{-1}cm^{-1}$-$10^{-3}cm^{-1}$, $V_Q\sim 10^{-3}cm^{-1}$

3. THE RESONANCE CONDITION FOR A FREE ION

Let the ion, having a total angular momentum $\vec{J}$, be placed in a constant external magnetic field $\vec{H}$. The spatial orientations of $\vec{J}$ are quantized and the energies of the levels associated with the

different orientations are $M_g\beta H$, where M is the electronic magnetic quantum number, g is the spectroscopic splitting factor, and β is the Bohr magneton. A high frequency magnetic field, polarized perpendicular to $\vec{H}$, will induce transitions between the levels, following the selection rule $\Delta M = \pm 1$, if the frequency of the field ν is such that the energy of the high frequency quanta is $h\nu = g\beta H$ ... 3.1

The population distribution of ions in thermal equilibrium with their surroundings is a Boltzmann one, so that the lower energy levels are more densely populated. Because upward and downward transitions have equal probability, it follows that the application of radiation will result in the tendency towards equality of the various level populations; this represents a net absorption of energy from the radiation field. If the sample is placed in a tuned circuit such as a cavity, this absorption of energy can be observed as a damping of the circuit.

4. THE CRYSTAL FIELD

In Section 3 the Hamiltonian for a free ion was considered. However, in practice we are not concerned with free ions and must take account of the ions' environment; i.e. the crystal lattice in which it is situated. The usual method of estimating the effect of the crystal in modifying magnetic properties is known as the crystalline field approximation. It is assumed that the influence of neighbouring ions occurs entirely through the electric field they produce at the magnetic ion site. Also it is assumed that surrounding ions are given a passive role and they are regarded as point charges which do not overlap the paramagnetic ion. The electrostatic potential at

the ion site, therefore obeys ... ce's equation $\nabla^2 V=0$. A complete set of solutions of this equation are the generalized Legendre polynomials. We may therefore expand the potential in terms of these polynomials, that is

$$V_e = \sum_n \sum_{m=-n}^{n} \sum_k A_n^m r^n Y_n^m(\theta_k \phi_k) = \sum_n \sum_m V_n^m$$

where the summation k is over all the electrons in the ion. We add this term to the equation (2.1) to give the general Hamiltonian for an ion in a crystal field: $\mathcal{H}=V_F+V_{LS}+V_{SS}+V_Z+V_Q+V_H+V_h+V_e$ .....(4.1)

In (4.1) V_F, V_Q and V_h are independent of the electronic spin. Therefore, if we neglect V_F, V_Q and V_h we obtain the electronic spin part of the Hamiltonian, called $\mathcal{H}_s = V_{LS}+V_{SS}+V_Z+V_H+V_e$

We can drop the spin-independent terms from $\mathcal{H}$, since they shift all levels equally and so do not enter into the energy differences.

5. THE SPIN-HAMILTONIAN FOR Gd^{3+} IN SINGLE CRYSTALS OF $YdCl_3.6H_2O$ $SmCl_3.6H_2O$ and $YCl_3.6H_2O$

The spin-Hamiltonian of Gd^{3+} in a single crystal of a rare-earth trichloride is given by[3]

$$\mathcal{H}=g\beta\vec{H}.\vec{S}+B_2^0O_2^0+B_2^2O_2^2+B_4^0O_4^0+B_4^2O_4^2+B_4^4O_4^4+B_6^0O_6^0+B_6^2O_6^2+B_6^4O_6^4+B_6^6O_6^6+\vec{S}.\vec{A}.\vec{I}. \quad ..(5.1)$$

with S=7/2. The O_l^m,s are spin operators which transform as the corresponding spherical harmonics, Y_l^m, and are given by the following expressions[4b]

$$O_2^0=3S_z^2-S(S+1) \qquad O_2^2=1/2(S_+^2+S_-^2)$$

$$O_4^0=35S_z^4-30S(S+1)S_z^2+25S_z^2-6S(S+1)+3S^2(S+1)^2$$

$$O_4^2 = 1/4\left[\left\{7S_z^2 - S(S+1) - 5\right\}(S_+^2 + S_-^2) + (S_+^2 + S_-^2)\left\{7S_z^2 - S(S+1) - 5\right\}\right]$$

$$O_4^4 = 1/2(S_+^4 + S_-^4)$$

$$O_6^0 = 231S_z^6 - 315S(S+1)S_z^4 + 735S_z^4 + 105S_z^2(S+1)^2 S_z^2 - 525S(S+1)S_z^2 + 294S_z^2 - 5S^3(S+1)^3 + 40S^2(S+1)^2 - 60S(S+1).$$

$$O_6^2 = 1/4\left[\left\{33S_z^4 - \left[18S(S+1)+123\right]S_z^2 + S^2(S+1)^2 + 10S(S+1) + 102\right\}(S_+^2 + S_-^2) + (S_+^2 + S_-^2)\left\{33S_z^4 - \left[18S(S+1)+123\right]S_z^2 + S^2(S+1)^2 + 10S(S+1) + 102\right\}\right]$$

$$O_6^4 = 1/4\left[\left\{11S_z^2 - S(S+1) - 38\right\}(S_+^4 + S_-^4) + (S_+^4 + S_-^4)\left\{11S_z^2 - S(S+1) - 38\right\}\right]$$

$$O_6^6 = 1/2(S_+^6 + S_-^6)$$

Here $S_+ = S_x + iS_y$ and $S_- = S_x - iS_y$

B_ℓ^m are coefficients dependent upon the crystal field and are determined by experiment. $\vec{\vec{A}}$ is the hyperfine splitting tensor.

The spin-Hamiltonian (5.1) can be separated into:

a. The fine-structure terms which describe the crystalline electric field splitting of the ground state of a paramagnetic ion. The fine-structure terms have the same symmetry properties as the crystalline electric potential at the site of the paramagnetic ion. In (5.1) the fine-structure terms are the ones involving Stevens operator-equivalents O_ℓ^m;

b. The hyperfine structure term $\vec{S}.\vec{\vec{A}}.\vec{I}$. which in the EPR spectrum is not normally observed since the linewidth usually obscures this structure; and

c. The first order Zeeman term $g\beta\vec{H}.\vec{S}$, where β is the Bohr magneton, $\vec{H}$ the magnetic field, g the spectroscopic splitting factor, and $\vec{S}$

the electron spin. The g-factor can be represented by its three principal values g_x, g_y and g_z, if the co-ordinate system is appropriately chosen. The g-factor is nearly isotropic for Gd^{3+} in most crystals since the ground state of Gd^{3+} is an orbital S-state to good approximation.

6. THE SPIN-HAMILTONIAN IN TENSOR FORM

The spin-Hamiltonian (5.1) can also be expressed in terms of tensor operators[3] $T_{\ell m}$ which are connected to the Stevens operator equivalents by the relation $O_\ell^m = \text{constant} \left[T_{\ell m} + (-1)^m T_{\ell,-m} \right]$

$$\mathcal{H} = g\beta H.S + B_{20}T_{20} + B_{40}T_{40} + B_{60}T_{60} + B_{22}\left[T_{22}+T_{2-2}\right] + B_{42}\left[T_{42}+T_{4-2}\right] + B_{62}\left[T_{62}+T_{6-2}\right] + B_{44}\left[T_{44}+T_{4-4}\right] + B_{64}\left[T_{64}+T_{6-4}\right] + B_{66}\left[T_{66}+T_{6-6}\right] \quad \ldots\ldots(6.1)$$

The relation between the B_ℓ^m of equation (5.1) and the $B_{\ell m}$ of equation (6.1) can best be exhibited through their connection with a new set of constants b_ℓ^m (in terms of which the computer calculations were performed) as given by the following:

$$b_2^0 = 3B_2^0 = \frac{\sqrt{6}}{2} B_{20} \qquad b_4^4 = 60B_4^4 = 30B_{44}$$

$$b_4^0 = 60B_4^0 = \frac{30}{\sqrt{70}} B_{40} \qquad b_6^2 = 1260B_6^2 = 315\sqrt{\frac{2}{11}} B_{62}$$

$$b_6^0 = 1260B_6^0 = \frac{315}{\sqrt{231}} B_{60} \qquad b_6^4 = 1260B_6^4 = 315\sqrt{\frac{6}{11}} B_{64}$$

$$b_2^2 = 3B_2^2 = 3B_{22} \qquad b_6^6 = 1260B_6^6 = 315B_{66}$$

$$b_4^2 = 60B_4^2 = \frac{60}{\sqrt{7}} B_{42}$$

$$b_4^4 = 60B_4^4 = 30B_{44} \qquad \ldots\ldots (6.2)$$

In terms of (5.2), the Hamiltonian becomes

$$\mathcal{H}=\beta\vec{H}.\vec{S}+1/3b_2^0O_2^0+1/60b_4^0O_4^0+1/1260b_6^0O_6^0+1/3b_2^2O_2^2+1/60b_4^2O_4^2+1/1260b_6^2O_6^2$$
$$+1/60b_4^4O_4^4+1/1260b_6^4O_6^4+1/1260b_6^6O_6^6+\vec{S}.\vec{A}.\vec{I} \qquad \ldots\ldots (6.3)$$

7. THE EQUATIONS FOR THE TRANSITIONS

For $H\|Z$, the transitions corresponding to $\Delta M=\pm1$ are given up to the second-order perturbation by[3]

$$\pm7/2\leftrightarrow\pm5/2 \quad E_\beta=h\nu\mp(6b_2^0+20b_4^0+6b_6^0)+E\left[\frac{45}{1\pm3F}-\frac{21}{1\pm5F}\right]$$
$$\pm5/2\leftrightarrow\pm3/2 \quad E_\beta=h\nu\mp(4b_2^0-10b_4^0-14b_6^0)+E\left[\frac{60}{1\pm F}-\frac{21}{1\pm5F}-\frac{45}{1\pm3F}\right]$$
$$\pm3/2\leftrightarrow\pm1/2 \quad E_\beta=h\nu\mp(2b_2^0-12b_4^0+14b_6^0)+E\left[\frac{21}{1\pm5F}-\frac{45}{1\pm3F}-\frac{120F}{1-F^2}\right]$$
$$+1/2\leftrightarrow-1/2 \quad E_\beta=h\nu+E\left[\frac{90}{1-9F^2}-\frac{120}{1-F^2}\right]$$

where $F=\dfrac{b_2^0}{5H}$ $\qquad$ $E=\dfrac{(b_2^2)^2}{15g\,H}$ $\qquad\ldots\ldots (7.1)$

b_2^0, b_4^0, b_6^0, and b_2^2 are the constants defined by (6.2)

Equation (5.1)(or (6.1)) can be used in principle to calculate the energy levels for any orientation of $\vec{H}$ with respect to the crystal axes. However, the calculations are extremely difficult if the dominant term $H_z=\mu\vec{H}.\vec{S}$ is not in the form HS_z. Therefore, one would like to rotate the axes so that $\vec{H}$ lies along the new z-direction. It is simpler yet to rotate the entire Hamiltonian instead. Then H_z becomes $\propto HS_z$ as desired; the problem then arises as to the transformation of the rest of the Hamiltonian. This problem was solved by Buckmaster et al[5] who gave the transformations for the tensor operators $T_{\ell m}$. Using their results the Hamiltonian becomes

$$\mathcal{H}=\beta(g_{\parallel}\cos^2\theta+g_{\perp}\sin^2\theta)HS_z+B_{20}(1/2(3\cos^2\theta-1)T_{20}+\sqrt{6}/2\sin\theta\cos\theta\left[T_{21}-T_{2-1}\right]+\sqrt{6}/4\sin^2\theta\left[T_{22}+T_{2-2}\right])+B_{40}(1/8(35\cos^4\theta-30\cos^2\theta+3)T_{40}+\sqrt{5}/4\sin\theta\cos\theta(7\cos^2\theta-3)\left[T_{41}-T_{4-1}\right]+\sqrt{10}/8\sin^2\theta(7\cos^2\theta-1)\left[T_{42}+T_{4-2}\right]+\sqrt{35}/4\sin^3\theta\cos\theta\left[T_{43}-T_{4-3}\right]+\sqrt{70}/16\sin^4\theta\left[T_{44}+T_{4-4}\right]+B_{60}(1/16(231\cos^6\theta-315\cos^4\theta+105\cos^2\theta-5)T_{60}+\sqrt{42}/16\sin\theta\cos\theta(33\cos^4\theta-30\cos^2\theta+5)\left[T_{61}-T_{6-1}\right]+\sqrt{105}/32\sin^2\theta(33\cos^4\theta-18\cos^2\theta+1)\left[T_{62}+T_{6-2}\right]+\sqrt{105}/16\sin^3\theta\cos\theta(11\cos^2\theta-3)\left[T_{63}-T_{6-3}\right]+3\sqrt{14}/32\sin^4\theta(11\cos^2\theta-1)\left[T_{64}+T_{6-4}\right]+3\sqrt{77}/32\sin^5\theta\cos\theta\left[T_{65}-T_{6-5}\right]+\sqrt{231}/32\sin^6\theta\left[T_{66}T_{6-6}\right])+B_{22}(\sqrt{6}/4\sin^2\theta T_{20}\mp1/2\sin\theta\left[(1\pm\cos\theta)T_{21}+(1\mp\cos\theta)T_{2-1}\right]+\frac{1}{4}\left[(1\pm\cos\theta)^2T_{22}+(1\mp\cos\theta)^2T_{2-2}\right])+B_{42}(\sqrt{10}/8\sin^2\theta(7\cos^2\theta-1)T_{40}\mp\sqrt{2}/8\sin\theta\left[(1\pm\cos\theta)(14\cos^2\theta\mp7\cos\theta-1)T_{41}+(1\mp\cos\theta)(14\cos^2\theta\pm7\cos\theta-1)T_{4-1}\right]+1/4\left[(1\pm\cos\theta)^2(7\cos^2\theta\mp7\cos\theta+1)T_{42}+(1\mp\cos\theta)^2(7\cos^2\theta\pm7\cos\theta+1)T_{4-2}\right]+14/8\sin\theta\left[(1\pm\cos\theta)^2(2\cos\theta\mp1)T_{43}-(1\mp\cos\theta)^2(2\cos\theta\pm1)T_{4-3}\right]+\sqrt{7}/8\sin^2\theta\left[(1\pm\cos\theta)^2T_{44}+(1\mp\cos\theta)^2T_{4-4}\right])+B_{44}(\sqrt{70}/16\sin^4\theta T_{40}\mp\sqrt{14}/8\sin^3\theta\left[(1\pm\cos\theta)T_{41}+(1\mp\cos\theta)T_{4-1}\right]+\sqrt{7}/8\sin^2\theta\left[(1\pm\cos\theta)^2T_{42}+(1\mp\cos\theta)^2T_{4-2}\right]\mp\sqrt{2}/8\sin\theta\left[(1\pm\cos\theta)^3T_{43}+(1\mp\cos\theta)^3T_{4-3}\right]+1/16\left[(1+\cos\theta)^4T_{44}+(1-\cos\theta)^4T_{4-4}\right])+B_{62}(\sqrt{105}/32\sin^2\theta(33\cos^4\theta-18\cos^2\theta+1)T_{60}\mp\sqrt{10}/32\sin\theta\left[(1\pm\cos\theta)(99\cos^4\theta\mp66\cos^3\theta-36\cos^2\theta\pm18\cos\theta+1)T_{61}+(1\mp\cos\theta)(99\cos^4\theta\pm66\cos^3\theta-36\cos^2\theta\mp18\cos\theta+1)T_{6-1}\right]+1/64\left[(1\pm\cos\theta)^2(495\cos^4\theta\mp660\cos^3\theta+90\cos^2\theta\pm108\cos\theta-17)T_{62}+(1\mp\cos\theta)^2(495\cos^4\theta\pm660\cos^3\theta+90\cos^2\theta\mp108\cos\theta-17)T_{6-2}\right]+3/32\sin\theta\left[(1\pm\cos\theta)^2(55\cos^3\theta\mp55\cos^2\theta+5\cos\theta\pm3)T_{63}-(1\mp\cos\theta)^2(55\cos^3\theta\pm55\cos^2\theta+5\cos\theta\mp
$$

$$\mp 3)T_{6-3}\Big] + \sqrt{30}/64\sin^3\theta\Big[(1\pm\cos\theta)^2(33\cos^2\theta\mp 22\cos\theta+1)T_{64}+(1\mp\cos\theta)^2(33\cos^2\theta\pm 22\cos\theta+1)T_{6-4}\Big] + \sqrt{165}/32\sin^3\theta\Big[(1\pm\cos\theta)^2(3\cos\theta\mp 1)T_{65}-(1\mp\cos\theta)^2(3\cos\theta\pm 1)T_{6-5}\Big] + 3\sqrt{55}/64\sin^4\theta\Big[(1\pm\cos\theta)^4T_{66}+(1\mp\cos\theta)^4T_{6-6}\Big]\Big)$$

$$+P_{64}\Big(3\sqrt{14}/32\sin^4\theta(11\cos^2\theta-1)T_{60}\mp 3/16\sin^3\theta\Big[(1\pm\cos\theta)(33\cos^2\theta\mp 11\cos\theta-2)T_{61}+(1\mp\cos\theta)(33\cos^2\theta\pm 11\cos\theta-2)T_{6-1}\Big] + \sqrt{30}/64\sin^2\theta\Big[(1\pm\cos\theta)^2(33\cos^2\theta\mp 22\cos\theta+1)T_{62}+(1\mp\cos\theta)^2(33\cos^2\theta\pm 22\cos\theta+1)T_{6-2}\Big]$$

$$+\sqrt{70}/32\sin\theta\Big[(1\pm\cos\theta)^3(11\cos^2\theta\mp 11\cos\theta+2)T_{63}+(1\mp\cos\theta)^3(11\cos^2\theta\pm 11\cos\theta+2)T_{6-3}\Big]+1/32\Big[(1\pm\cos\theta)^4(33\cos^2\theta\mp 44\cos\theta+13)T_{64}+(1\mp\cos\theta)^4(33\cos^2\theta\pm 44\cos\theta+13)T_{6-4}\Big]+\sqrt{22}/32\sin\theta\Big[(1\pm\cos\theta)^4(3\cos\theta\mp 2)T_{65}-(1\mp\cos\theta)^4(3\cos\theta\pm 2)T_{6-5}\Big] + \sqrt{6}/64\sin^2\theta\Big[(1\pm\cos\theta)^4T_{66}+(1\mp\cos\theta)^4T_{6-6}\Big]\Big)$$

$$+P_{66}\Big(\sqrt{231}/32\sin^6\theta P_{60}\mp 3\sqrt{22}/32\sin^5\theta\Big[(1\pm\cos\theta)T_{61}+(1\mp\cos\theta)T_{6-1}\Big] + 3\sqrt{3}/64\sin^4\theta\Big[(1\pm\cos\theta)^2T_{62}+(1\mp\cos\theta)^2T_{6-2}\Big] + \sqrt{55}/32\sin^3\theta\Big[(1\pm\cos\theta)^3T_{63}+(1\mp\cos\theta)^3T_{6-3}\Big] + \sqrt{66}/64\sin^2\theta\Big[(1\pm\cos\theta)^4T_{64}+(1\mp\cos\theta)^4T_{6-4}\Big] + \sqrt{3}/32\sin\theta\Big[(1\pm\cos\theta)^5T_{65}+(1\mp\cos\theta)^5T_{6-5}\Big]+1/64\Big[(1\pm\cos\theta)^6T_{66}+(1\mp\cos\theta)^6T_{6-6}\Big]\Big) \quad \ldots\ldots\ldots\ldots\ldots\ldots\ldots\ldots\ldots\ldots\ldots\ldots(7.2)$$

Equation (7.2) is formally the same as (6.1), if one groups the $P_{\ell m}$'s and the trigonometric function to define new θ-dependent $P'_{\ell m}$'s. Then, equation (7.1) may again be used to give the new resonance frequencies, where (6.2) defines the θ-dependent b^m_ℓ's.

Substitution of $\theta = 90^\circ$ into equation (7.2) gives the Hamiltonian for the external field in the x-direction. Therefore for H||X equation (5.1) becomes

$$\mathcal{H}=\mu_B \beta H S_z + \left[-1/2B_2^0+1/2B_2^2\right]O_2^0+\left[3/8B_4^0-1/8B_4^2+1/8B_4^4\right]O_4^0+\left[-5/16B_6^0+1/16 B_6^2-1/16B_6^4+1/16B_6^6\right]O_6^0+\left[-3/2B_2^0-1/2B_2^2\right]O_2^2+\left[5/2B_4^0-1/2B_4^2-1/2B_4^4\right]O_4^2 \quad ..(7.3)$$

where only those terms which give diagonal and appreciable off-diagonal elements have been retained.

As an illustration of the remarks made after equation (7.2), one sees that equation (7.3) looks like equation (5.1) if we define $(E_2^0)_x = (-1/2B_2^0+1/2B_2^2)$ and so on.

8. CONVERSION FACTORS FOR b_ℓ^m's

The fine structure parameters b_ℓ^m may be expressed in units of wave number (cm^{-1}), of frequency (GHz, MHz), or of magnetic field (Tesla, Gauss). The conversion relations are[3]

$$b_\ell^m(GHz)=10^{-3}\times b^m(MHz)=29.97925\times b_\ell^m(cm^{-1})$$

$$b_\ell^m(GHz)=g\times 13.99600\times b^m(T)=g\times 13.99600\times 10^{-4}\times b_\ell^m(G)$$

where g is the spectroscopic splitting factor.

9. MEASUREMENT OF MICROWAVE FREQUENCY

The measurement of the microwave frequency can be done by placing a DPPH marker into the cavity together with the crystal. Knowing the magnetic field for the DPPH transition, equation (3.1) can be used, with $g=2.003$ the spectroscopic splitting factor for DPPH.

CHAPTER III

APPARATUS

The apparatus used for experimental work on Gd^{3+} in $NdCl_3.6H_2O$ $YCl_3.6H_2O$ and $SmCl_3.6H_2O$ was the paramagnetic resonance spectrometer assembled by G. E. Sharp.[6] A block diagram of the spectrometer is shown in Fig. 1, page 34. A description of the various parts is as follows.

1. THE MICROWAVE SOURCE

The microwave source is a forced air-cooled Varian X-13 reflex klystron with a frequency range of 8.1 to 12.4 GHz and a power rating of 180 mw. A Hewlett-Packard model 715A power supply produces the required beam voltage of +400 volts d.c. with a ripple of less than 7 mv and a beam current of 50 ma. A wide range of reflector voltages from 0 to -300 volts d.c. with respect to the beam supply are available with a ripple of less than 10 mv. The filament voltage supply provides 1.5 amps at 6.3 volts a.c.

2. THE WAVEGUIDE NETWORK

The DeMornay-Bonardi model DBG-480 isolator permits the transmission of microwaves in one direction and prevents their transmission in the opposite direction. This prevents the waveguide network from acting back on, and influencing, the frequency stability of the klystron.

In order to measure the frequency of operation, ten percent of microwave power is coupled off to a Hewlett-Packard model 532 wave meter with a dial accuracy of .05 percent. The microwave

power is detected by a Hewlett-Packard model X424A crystal detector. The resonance frequency is indicated on the scope when a dip in the transmitted power is observed.

A Hewlett-Packard model 382 calibrated attenuator is placed between the load and the generator to reduce the signal intensity incident upon the load. This is adjusted to give optimum signal-to-noise ratio.

The required power from the attenuator enters arm 3 of the DeMornay-Bonardi model DBG-650 magic tee (Fig. 1, page 34), where the power splits between arms 1 and 2. Arm 2 is the cavity arm (to be discussed in the next section). Arm 1 is made up of a Hewlett Packard model 870A slide screw tuner and a Hewlett model 914B matched load. A slide screw tuner is used to produce an under-coupled cavity match because the crystal detector operates more efficiently with a definite amount of power incident at all times. Arm 4 is the detector arm to which is connected a Hewlett Packard model 485B detector mount containing a IN23D silicon diode which provides a good signal-to-noise ratio.

3. THE SAMPLE CAVITY

Fig2,p35 shows a detailed view of the cavity arm of the spectrometer. The cavity, which is gold plated, is a rectangular type, resonating in the TE_{102} mode at a frequency of 9.46 GHz to wavemeter accuracy. The generalized relationship for the wavelength in a uniform rectangular waveguide operating in the TE_{10n} mode is

$$1/\lambda_g^2 = 1/\lambda_0^2 + 1/\lambda_c^2$$

where λ_g = guide wavelength

λ = free space wavelength = c/f

λ_c = cutoff wavelength = 2a, where a is the broad dimension of the rectangle.

For a resonant frequency of 9.5 GHz, the guide wavelength turns out to be 4.361 cm. Due to a difference of .54 mm after machining and gold-plating, the resonant frequency of the cavity is 9.46 GHz.

The cavity is coupled to the waveguide by a .010 inch gold-plated sheet with an iris of .2 inch diameter. The cavity is matched to the waveguide by a .030 inch inductive pin. The pin is connected to a cam and rod which leads to the flange of the cryostat.

The cavity, iris and mounting for the tuner are connected to a flange at the end of a ten inch brass waveguide by four machine screws. The waveguide is chosen to be of brass in order to add weight to reduce cavity vibrations.

4. FREQUENCY STABILIZER

A Micro-Now model 210 cavity stabilizer is used to provide the frequency stabilization for a wide variety of microwave frequencies. Stabilization is performed by FM discrimination of an external reference cavity (or wavemeter) and thus absolute stability is a function of the reference cavity Q.

5. THE DETECTING AND AMPLIFYING SYSTEM

The crystal detector demodulates the microwave power, which is then transferred by a coaxial cable to the Princeton Applied Research model 122 lock-in amplifier. This instrument enables the rms value of the fundamental frequency component to be measured accurately.

The basic element of the amplifier is a phase sensitive detector in which the signal voltage is mixed with a reference voltage, producing sum and difference frequencies. A low pass filter at the output of the mixer rejects the high frequency components corresponding to the sum-frequencies and passes the difference frequencies which lie in the frequency band which are allowed to pass. The difference frequencies from components of the signal spectrum which differ from the reference frequency by more than the cut-off frequency of the low pass filter are attenuated. Consequently the output of the low pass filter will be due to that portion of the signal spectrum which lies about the reference frequency within a pass-band determined by the low pass filter.

The front panel "monitor" switch allows one of the outputs of the signal amplifier, the output of the reference tuned amplifier, or the output of the dc amplifier to appear at both the monitor jack (for display) and the meter. The sensitivity of the signal channel can be varied from .1mV to 50.0 mV. The time constants can also be varied from 1 msec to 30 sec. A time constant of 1 sec gives the best signal-to-noise ratio for the derivative of the absorption curve.

The reference channel can be tuned over a frequency range of 5Hz to 150kHz of a continuous front panel control. There is a continuously adjustable phase shifter with a range of 0° to 360° phase shift as well.

The resulting dc output from the lock-in-amplifier is plotted on a Moseley model 7005A servo potentiometer X-Y recorder. Each

axis of the recorder has an independent servo system with no interaction between channels. The X-axis is driven by a fraction of the signal provided by the X-axis drive of the Varian field dial used to regulate and sweep the magnetic field. The Y-axis is driven by the output of the lock-in-amplifier, thus yielding a plot of the derivative of the absorption versus magnetic field.

6. PRODUCTION OF MAGNETIC FIELDS

The magnetic field H is provided by a Varian V-3900 electromagnet which is capable of producing a field of 13 kG across a 3 inch magnet gap. The center of each pole piece contains a .50 inch hole for the purpose of irradiating samples when radiation is incident in the longitudinal direction with respect to the magnetic field. The pole pieces are equipped with shims to produce a homogeneous field.

The Varian 10-kW VFR-2503 control unit has digital field control dials with increments of .10 G which assures accurate field settings. The control panel also includes a field reversing switch, a test selection switch, a meter to monitor the magnet system operation and a complete linear sweep. Sweep ranges from .25 G to 10 kG with sweep times of .50 min to 100 min can be selected. A temperature controlled Hall-effect crystal probe mounted on one magnet pole cap maintains the magnetic field within one percent of the selected field value.

7. MAGNETIC FIELD MEASUREMENTS: THE GAUSSMETER

The magnetic field can be measured either by taking the reading

from the digital field control dial or, for greater accuracy, by using the nuclear magnetic resonance probes containing protons for fields of 1 kG to 8 kG and deuterons from 8 kG to 10 kG. The magnetic field for lines below 1 kG can be taken from a calibration curve which can be plotted using the magnetic field measurements in the range 1 kG to 10 kG.

The Gaussmeter is an instrument using the nuclear magnetic resonance principle (NMR), and is used to measure and calibrate magnetic fields. The instrument used to make these measurements was a Varian F-8 nuclear fluxmeter and a Hewlett-Packard model 5245n frequency counter. Neglecting the effect of an inhomogeneous magnetic field, the probable error is .0038 percent which is constant throughout the range of the fluxmeter.

8. THE MAGNETIC FIELD MODULATION

The magnetic field is modulated at a frequency of 390 Hz using a sinusoidal sweep small compared to the dc magnetic field. The modulation amplitude is adjusted to give a good representation of the desired derivative. The pair of coils is wrapped in a masonite form and rigidly mounted on the magnet pole pieces. Each coil is 90 turns of number 12 insulated copper wire. These were connected in series with a 30 F capacitor to the power supply. A Hewlett Packard model 204C oscillator supplied the sinusoidal signal. The amplifier is capable of producing 100 watts rms, the maximum current being 2 amps ac rms.

9. PRINCIPLE OF DETECTION

The cavity is tuned so that all available power from the klystron

is absorbed by the cavity when the resonance occurs at a given frequency, the frequency being dependent upon the dimension of the cavity. When the frequency of the microwave field and the amplitude of the magnetic field satisfy the resonance condition of the sample, the impedance of the cavity is such that a signal is reflected to the crystal detector in the hybrid tee.

Fig. 3(a), page 36 represents the change in output of the detector at resonance as a simple function of the steady magnetic field at the sample. Fig. 3(b), page 36 shows the variation of the sinusoidal field as a function of time and Fig. 3(c), page 36 shows how the static curve translates these variations into a time-varying signal as the output of the microwave detector. The signal at the output of the amplifier varies in time in the manner indicated in Fig. 3(d), page 36. The change in the sign of the derivative of the absorption curve is conveyed in the waveform of Fig. 3(d) as a reversal in phase relative to the field modulation waveform. The waveform at the output of the amplifier enters the phase sensitive detector that used the original sinusoidal waveform as reference. The dc output of the detector is a representation of the derivative of the absorption line as shown Fig. 3(e), page 36.

CHAPTER IV

COMPUTER ANALYSIS OF EPR DATA

The calculation of the spin-Hamiltonian parameters can be done using digital computing procedures.[7]

The object of this chapter is to demonstrate how the adjustable parameters in the spin-Hamiltonian can be evaluated using a computer.

An iterative and convergent computing procedure has been used for evaluating the "best-fit" adjustable parameters in the generalized spin-Hamiltonian from experimental EPR spectra.

1. DESCRIPTION OF THE COMPUTATION PROCEDURE

The procedure for calculating the spin-Hamiltonian parameters is based on a standard digital computer sub-routine for exactly diagonalizing symmetric matrices with real or complex elements, and is completely general since it is applicable to any generalized spin-Hamiltonian.

The computer procedure is more useful than perturbation methods for determining spin-Hamiltonian parameters because the exact diagonalization of the matrix is not limited by any assumption concerning the relative magnitude of the terms in the spin-Hamiltonian.

The secular determinant of a spin-Hamiltonian must be formed before the spin-Hamiltonian parameters can be determined. The spin-Hamiltonian expressed in terms of Stevens operators or tensor operators can be used. The matrix elements for the Stevens operators are tabulated in many textbooks[4b] and are used in this work for this reason.

The eigenvalues of the spin-Hamiltonian can be obtained by solving its secular determinant when the values of parameters in the spin-Hamiltonian are provided.

The N observed $\Delta M=\pm 1$ transitions for a system of M+1 energy levels are assumed to occur at magnetic field values B_j, j=1,2 ..,N, where B_j corresponds to the $|M/2+1-j\rangle \leftrightarrow |M/2-j\rangle$ transition, and the resonant frequency of the sample cavity during the measurement of the B_j is ν. The values of ν and B_j(j=1,2 ..,N) constitute the experimental part of the input data set. The measurement accuracy with which the parameters in any generalized spin-Hamiltonian have been determined, are consistent with the input data set.

The steps in the computational procedure are now given. A series of synthetic transitions are constructed and a least-squares criterion is employed to obtain a convergent sequence for determining the best-fit adjustable parameters in a spin-Hamiltonian.

1. The magnitude of the adjustable parameter P_i appearing in the generalized spin-Hamiltonian to which the input data set is to be fitted are estimated. These estimates are not critical because initial errors will be corrected at later stages in the computation.

2. The parameters are arranged in decreasing order of magnitude so that P_1 is the largest, P_2 is the second largest, etc.

3. The initial value for each parameter P_i, $P_{i,o}$, is chosen.

4. A searching range for each parameter is chosen within which the best-fit value of the parameter is expected to lie. The extent of the range is determined by the confidence with which the initial

values $P_{i,o}$ were chosen.

5. Each searching range is divided into nine steps. The initial trial values of each P_i are labelled $P_{i,k}$ where k=1,2 ..,10.

6. The calculation is commenced by setting the values of the parameters P_i, $i \neq 1$ at $P_{i,o}$. The secular determinant is diagonalized for each magnetic field value B_j(j=1,2, ..,N) for each of the ten values of $P_{1,k}$(k=1,2, ..,10). In total, 10N diagonalizations are performed.

7. The eigenvalues for each diagonalization are arranged in decreasing order of magnitude and labelled $E^m_{j,k}$(m=1,2, ..,N-1). The energy differences corresponding to $\Delta^\ell = \pm 1$ transitions are calculated using $\Delta E^\ell_{j,k} = E^{(\ell+1)}_{j,k} - E^\ell_{j,k}$ (ℓ=1,2, ..,N).

8. The j^{th} value of $\Delta E^\ell_{j,k}$, $E^j_{j,k}$, is compared with the observed energy difference which is proportional to the measured microwave frequency. For each value of $P_{1,k}$, there are N values of $E^j_{j,k}$ which form a calculated spectrum. The mean-square-deviation (MSD) of each calculated spectrum is determined using

$$MSD_k = \sum_{j=1}^{N} (E^j_{j,k} - CV)^2$$ where C is constant.

C=1 if the frequency and the parameters are expressed in the same unit. The unit of GHz (10^9Hz) is the most convenient to be used. The minimum of MSD_k, $(MSD_k)_{min}$, determines the best-fit value of $P_{1,k}$, $(P_{1,k})_{min}$.

9. Steps (6) to (8) are repeated for $P_{2,k}$ using $(P_{1,k})_{min}$ and $P_{i,o}$ where $i \neq 1$ or 2.

10. Step (9) is repeated until all the initial values of the parameters $P_{i,o}(i=1,2,..)$ have been replaced by $(P_{i,k})_{min}$

11. The searching range of each parameter is reduced by a convergent factor which determines the convergence rate of the computations. Steps (5) to (10) are repeated using the reduced searching ranges.

12. The iteration process described in step (11) is repeated until the MSD is reduced to a value consistent with the accuracy of the experimental data.

A diagram outlining the above steps in the procedure is given in Fig. 4, page 37.

2. SAMPLE CALCULATION

A sample calculation is given to illustrate the computation procedure described above. It will be the calculation of the spin-Hamiltonian parameters for Gd^{3+} in $SmCl_3.6H_2O$ from our data.

The sample analysis is carried out for the magnetic field parallel to the crystal symmetry axis and for the case where only six parameters are considered, as exhibited by the Hamiltonian

$$\mathcal{H}=\beta_e\vec{H}.\vec{S}+1/3b_2^0O_2^0+1/3b_2^2O_2^2+1/60b_4^4O_4^4+1/60b_4^0O_4^0+1/1260b_6^0O_6^0$$

Input Data:

(i) Microwave frequency ν=9.4432562GHz

(ii) Magnetic flux density orientation $\theta=0^o$.

(iii) Magnetic flux density of EPR transitions $B_j(j=2,..,7)$

.0820T; .21615T; .3500T; .4813T; .6055T; .7111T (T=Tesla)

(iv) Initial estimated values and searching ranges of the g-value

and fine structure spin-Hamiltonian parameters

Input Data:

	g	b_2^0(GHz)	b_2^2(GHz)	b_4^4(GHz)	b_4^0(GHz)	b_6^0(GHz)
Initial estimated values	1.99	1.8	-1.1	.095	-.03	-.0005
Initial searching ranges						
Starting value	1.883	1.749	-1.263	.0908	-.0392	-.0013
Increment	.015	.01	.01	.01	.001	.0001

Output Results:

Fittings	g	b_2^0(GHz)	b_2^2(GHz)	b_4^4(GHz)	b_4^0(GHz)	b_6^0(GHz)
First	1.973	1.809	-1.203	.0968	-.0332	-.0007
Second	1.991	1.821	-1.191	.098	-.032	-.00058
Third	1.994	1.823	-1.1886	.0982	-.0317	-.00056

etc.

Note: The initial values were obtained from a perturbation calculation.

CHAPTER V

EXPERIMENTAL PROCEDURE

1. CRYSTALLOGRAPHY AND SAMPLE PREPARATION

$NdCl_3.6H_2O$ is a monoclinic[8] crystal with $\beta=93^o$, a=9.72 Å b=6.6 Å and C=7.9 Å. $YCl_3.6H_2O$ is a monoclinic crystal[9] with $\beta=93.6^o$. $SmCl_3.6H_2O$ is a monoclinic crystal[10] with $\beta=93^o\ 40'$, a=9.6 Å, b=6.61 Å and C=8.0 Å.

In Fig. 5, page 38, is shown a monoclinic crystal[9] for the $NdCl_3.6H_2O$ $SmCl_3.6H_2O$ and $YCl_3.6H_2O$. The magnetic axes also are shown.

The crystals used for this work were grown in this laboratory from solutions of $GdCl_3.6H_2O$ and $NdCl_3.6H_2O$ and $SmCl_3.6H_2O$ and $YCl_3.6H_2O$. The proportions by weight are

$$\frac{Gd}{Nd}=\frac{1}{100} \text{ and } \frac{Gd}{Y}=\frac{1}{100} \text{ and } \frac{Gd}{Sm}=\frac{1}{100}$$

The crystals had to be grown in a dry place with no water vapor, otherwise as soon as they formed they liquify again. For this reason they were put in varnish as soon as they were grown.

2. FINDING THE SPECTRA

From the shape of the crystal it was possible to see which way it should be mounted in the cavity so that the magnetic field would be in the ZX-plane. After getting the spectrum the crystal was turned round a little and the process repeated, making sure that it was mounted exactly on the plane desired.

3. ANGULAR VARIATION OF SPECTRA

When the exact plane was known for which the crystal was mounted

the angular variation from 0^{o} to 90^{o} with respect to the Z-axis was observed. The spectra of the $NdCl_3.6H_2O$ for H along the Z-axis and X-axis are given by Figs. 6, page 39, and 7, page 40, respectively. The spectra of the $YCl_3.6H_2O$ for H along the Z-axis and X-axis are given by Figs. 8, page 41, and 9, page 42, respectively. The spectra of the $SmCl_3.6H_2O$ for H along the Z-axis and X-axis are given by Figs. 10, page 43 and 11, page 44 respectively.

The EPR angular spectra of $\Delta m=\pm 1$ transitions of the Gd^{3+} ion in $SmCl_3.6H_2O$, $NdCl_3.6H_2O$ and $YCl_3.6H_2O$ were measured at 2^{o} intervals in the XZ-plane. The results are given in tables I, II and III, pages 45, 46 and 47 and Figs. 12, 13 and 14, pages 48, 49 and 50 show the angular spectra of Gd^{3+} in $SmCl_3.6H_2O$, $NdCl_3.6H_2O$ and $YCl_3.6H_2O$ respectively. In Tables I, II and III there are omissions in some columns. The entries are not made because the change in value from neighbouring orientations is small.

CHAPTER VI

SPIN-HAMILTONIAN PARAMETERS

The spin-Hamiltonian (6.3) was employed in the analysis of EPR spectra of Gd^{3+} in $SmCl_3.6H_2O$, $NdCl_3.6H_2O$ and $YCl_3.6H_2O$. The secular determinant of the spin-Hamiltonian is given in Appendix I, page 51.

The facilities of the Time-Sharing-System of the Computer Center at Sir George Williams University as well as these of Sigma 7 computer at Harvard University were used for calculations. The computer procedure outlined in Chapter IV was used and the programme is given in Appendix II, pages 52-57, which also contains the sub-routine for the diagonalization of the Hamiltonian.

The parameters of the spin-Hamiltonian obtained are given below. The values in parentheses are those obtained by previous workers[8-10].

a. Gd^{3+} in $SmCl_3.6H_2O$

$g_{\parallel}$ =1.991 (1.99) $g_{\perp}$ =1.9818 (1.99) b_2^0=1.8441GHz (1.8588)

b_4^0=-.0317GHz (-.0329) b_2^2=-1.118GHz (-1.1849) b_6^0=-.00055GHz (-.00245)

b_4^2=-.0254GHz b_4^4=.0983GHz b_6^2=.00068GHz b_6^4=.03188GHz

b_6^6=-.00359GHz ; [$b_4^4-b_4^2$=.1237GHz (.1358)

$b_6^6-b_6^4+b_6^2$=-.03477GHz (-.03297)]

b. Gd^{3+} in $NdCl_3.6H_2O$

$g_{\parallel}$ =1.99237 (1.987) $g_{\perp}$ =1.98249 (1.986) b_2^0=1.86298GHz (1.834)

b_4^0=-.0317GHz (-.0329) b_6^0=-.00055GHz (-.00125)

b_2^2=-1.09912GHz (-1.152) b_4^2=-.02537GHz b_4^4=.0983GHz

b_6^2=-.00069GHz b_6^4=.023GHz. b_6^6=-.00415GHz ;$\left[b_4^4-b_4^2\right.$=.12367GHz (.1359)

$b_6^6-b_6^4+b_6^2$=-.02784GHz (-.02406)$\left.\right]$

c. Gd^{3+} in $YCl_3.6H_2O$

$g_{\parallel}$ =1.994 (1.999) $g_{\perp}$ =1.98247 (1.988) b_2^0=1.89121GHz (1.6009)

b_4^0=-.03088GHz (-.009) b_2^2=-1.11855GHz (2.3024)

b_6^0=.00003GHz b_4^2=-.01658GHz b_4^4=.09898GHz b_6^2=-.00214GHz

b_6^4=.02294GHz b_6^6=-.00408GHz

DISCUSSION

The generalized spin-Hamiltonian parameters for Gd^{3+} ion in $SmCl_3.6H_2O$, $NdCl_3.6H_2O$ and $YCl_3.6H_2O$ were calculated. By using the computer "best-fit" value method the parameters were calculated more accurately than would be obtained using perturbation theory where small terms are neglected compared with large terms. With this method all the parameters can be calculated individually in contrast to the perturbation theory where some of the parameters can only be calculated as linear combinations of two or three.

In the previous section the results were given together with

the results by previous workers. It has been seen that the spin-Hamiltonian parameters calculated in this work predict the position of the lines much more accurately than those obtained by others.

We calculated a parameter $MSD=\sum_{j=1}^{N}(\Delta E_j - h\nu)^2$ to test this; here $h\nu$ is the energy of the microwave quanta and ΔE_j are the calculated energy differences at a given resonant magnetic field. The following values of MSD were obtained:

Host	MSD $(GHz)^2$
$NdCl_3.6H_2O$	.03653288
$SmCl_3.6H_2O$	.15542364
$YCl_3.6H_2O$	.00556770

The b's of this work for Gd^{3+} in $SmCl_3.6H_2O$ and $NdCl_3.6H_2O$ are not very different from the ones given by Singh et al[10]. But for the case of Gd^{3+} in $YCl_3.6H_2O$ Meierling et al[9] gives only b_2^0, b_4^0 and b_2^2 since they do not use the complete spin-Hamiltonian for orthorombic or lower site symmetry. The numerical values of their b's differ widely from ours.

The g-value observed in this work is of the order of 1.991-1.994 which is less than that of the free electron g-value. This deviation in g-value in the case of Gd^{3+} has been explained theoretically by Lacroix[11] who calculated the g-value for the ground state $^8S_{7/2}$ of Gd^{3+} by considering perturbations due to the excited states through the spin-orbit coupling $\zeta\sum_i \vec{l}_i.\vec{s}_i$. He obtained a g-value of 1.9930 by taking into account the $^6P_{7/2}$ excited state assuming that the value of the spin-orbit coupling constant ζ was 1540 cm^{-1}.

Wybourne[12] obtained a g-value of 1.99454 for the ground state using a best-fit value for ζ.

It should be noted that the closer the g-values are to the free ion value, the less admixture there is of excited states (e.g. p-states) to the ground s-states.

Furthermore, the following comments on the g-values can be made:

a. Gd^{3+} in $SmCl_3.6H_2O$

$\Delta g_{\parallel} = .0113$ (.0123) (where $\Delta g_{\parallel}$ stands for the deviation of the g-value from that of the free ion). The value in parenthesis is that given by Singh et al[10]. $\Delta g_{\perp} = .0205$ (.0123). What we notice here is that our $g_{\parallel} \neq g_{\perp}$ which implies anisotropy in g-value, is in contrast to that given by Singh et al[10] $g_{\parallel} = g_{\perp}$.

b. Gd^{3+} in $NdCl_3.6H_2O$

$\Delta g_{\parallel} = .0100$ (.0153) and $\Delta g_{\perp} = .01981$ (.0163)

Here again our $g_{\parallel}$ is closer to the free ion value than that of reference 8. Also the anisotropy of our g-value is greater than the one given by Singh et al[8].

c. Gd^{3+} in $YCl_3.6H_2O$

$\Delta g_{\parallel} = .0083$ (.0033) and $\Delta g_{\perp} = .01983$ (.0143)

Here the $g_{\parallel} = 1.999$ of reference 9 is in better agreement with that of the free ion than our value $g_{\parallel} = 1.994$. Again the anisotropy of our g-value is greater than that of reference 9. The fact that Meierling et al[9] get a closer value of $g_{\parallel}$ to that of a free ion can be a result of their not using the full spin-Hamiltonian.

In conclusion, it can be said that there is a very small

$^6P_{7/2} - {}^8S_{7/2}$ admixture in all the cases. The values of $g_{\parallel}$ are in good agreement with those calculated by Lacroix[11]. There are, however, no calculations available for $g_{\perp}$ to be compared with our experimental values.

The hyperfine structure corresponding to the odd isotopes (155,157) of Gd^{3+} was not observed. This is probably because the fine structure lines are quite broad (60-150) gauss while the hyperfine structure constant reported by earlier workers[10] is only about 4 to 6 gauss.

CHAPTER VII
CONCLUSION

The electron paramagnetic resonance of Gd^{3+} doped in $SmCl_3.6H_2O$, $NdCl_3.6H_2O$ and $YCl_3.6H_2O$ was studied at room-temperature, by varying the magnetic field in the XX-plane of each crystal.

The spin-Hamiltonian parameters were estimated from the resulting values of the static magnetic field using an iterative and convergent computing procedure. This method gave us the best-fit values of all the parameters individually.

A definite anisotropy of the g-value was observed in all the three hosts in contrast with the isotropic values found by Singh et al[10] for Gd^{3+} in $SmCl_3.6H_2O$.

The g values of Gd^{3+} doped in $SmCl_3.6H_2O$, $NdCl_3.6H_2O$ and $YCl_3.6H_2O$ were found to lie close to the values theoretically calculated by Lacroix[11] and by Wybourne[12]

It was concluded that since our g-values are not the same as those for a free ion, there is $^6P_{7/2} - {}^8S_{7/2}$ admixture present. However, since the difference for the free ion g-value is not large, this admixture should be quite small.

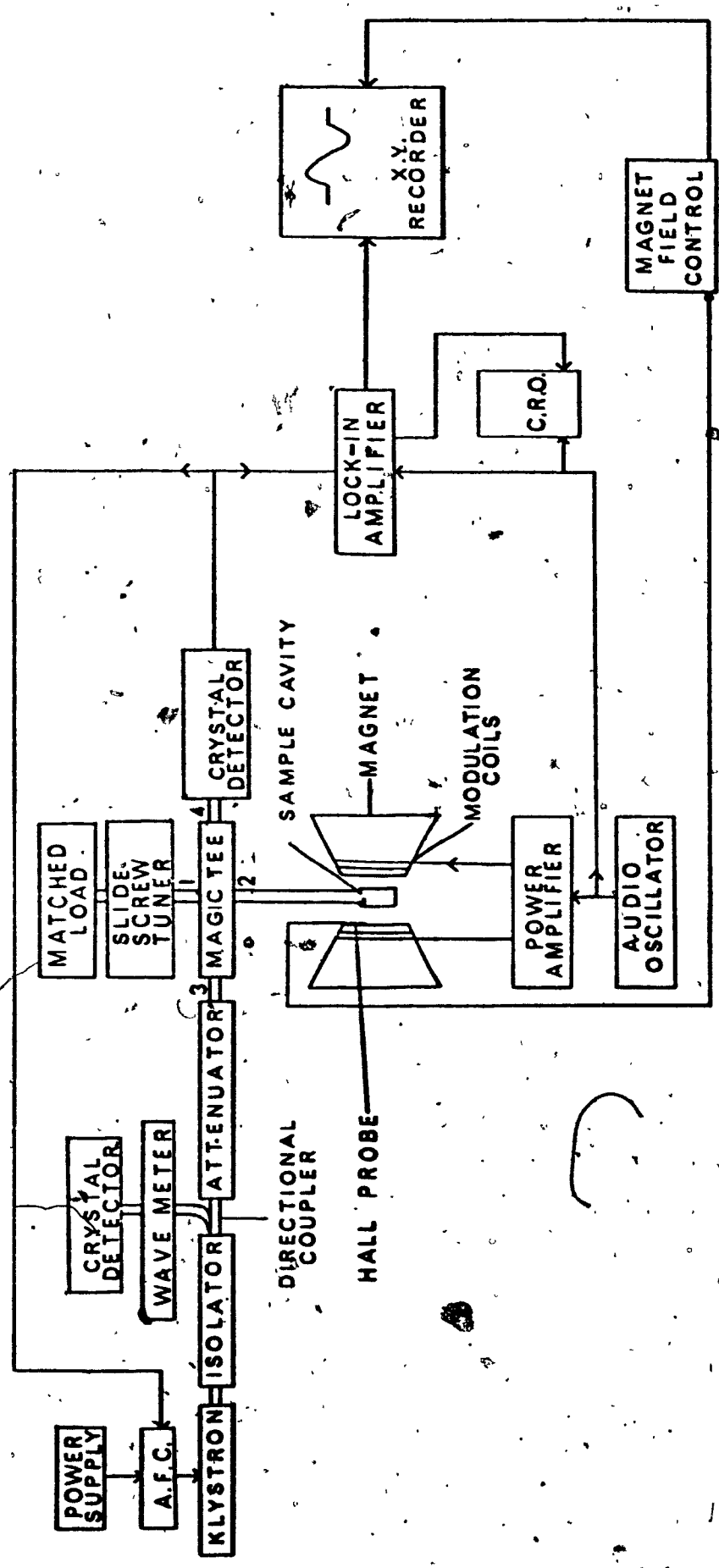

Fig. 1. Block diagram of the X-band spectrometer

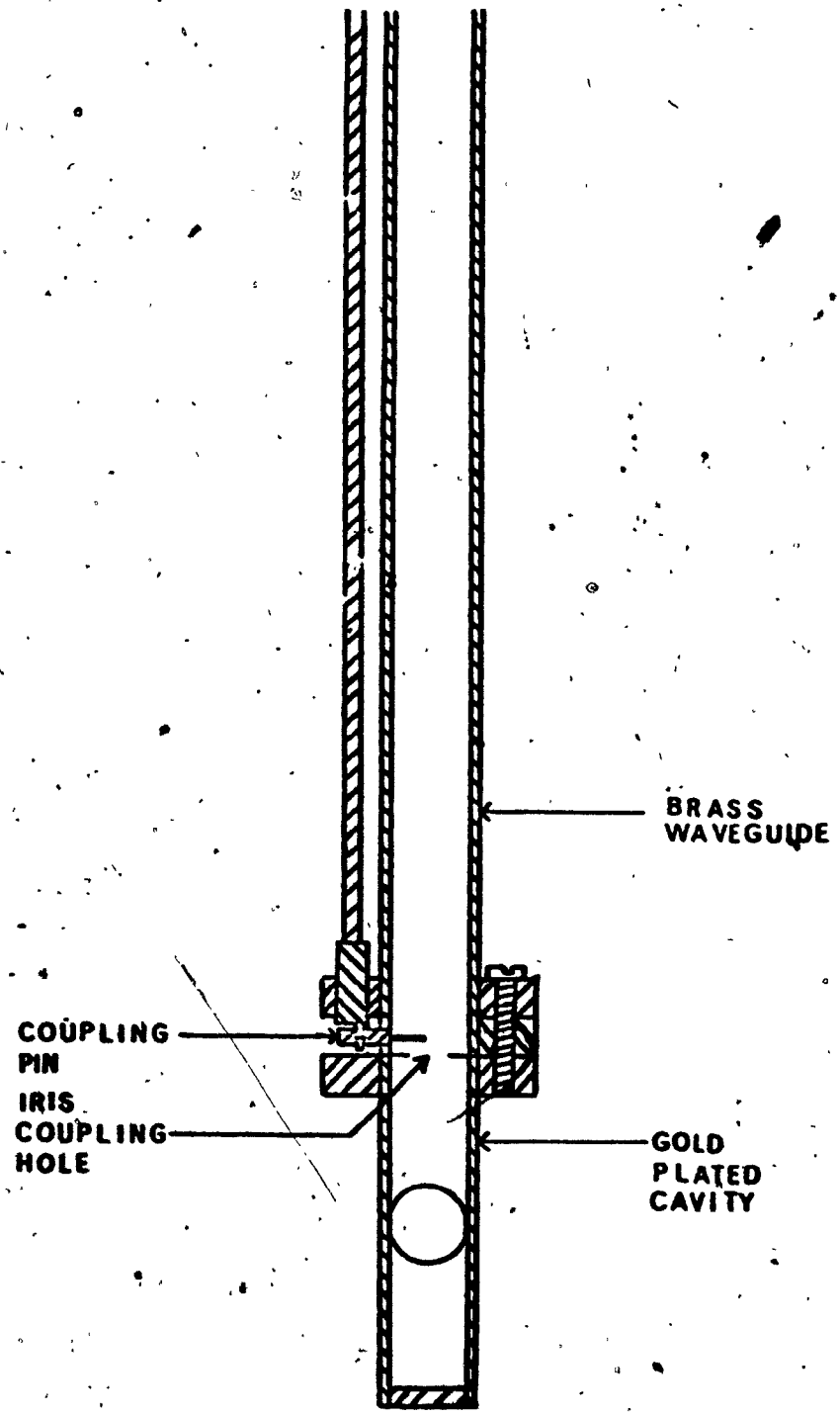

Fig. 2 Detailed view of cavity arm

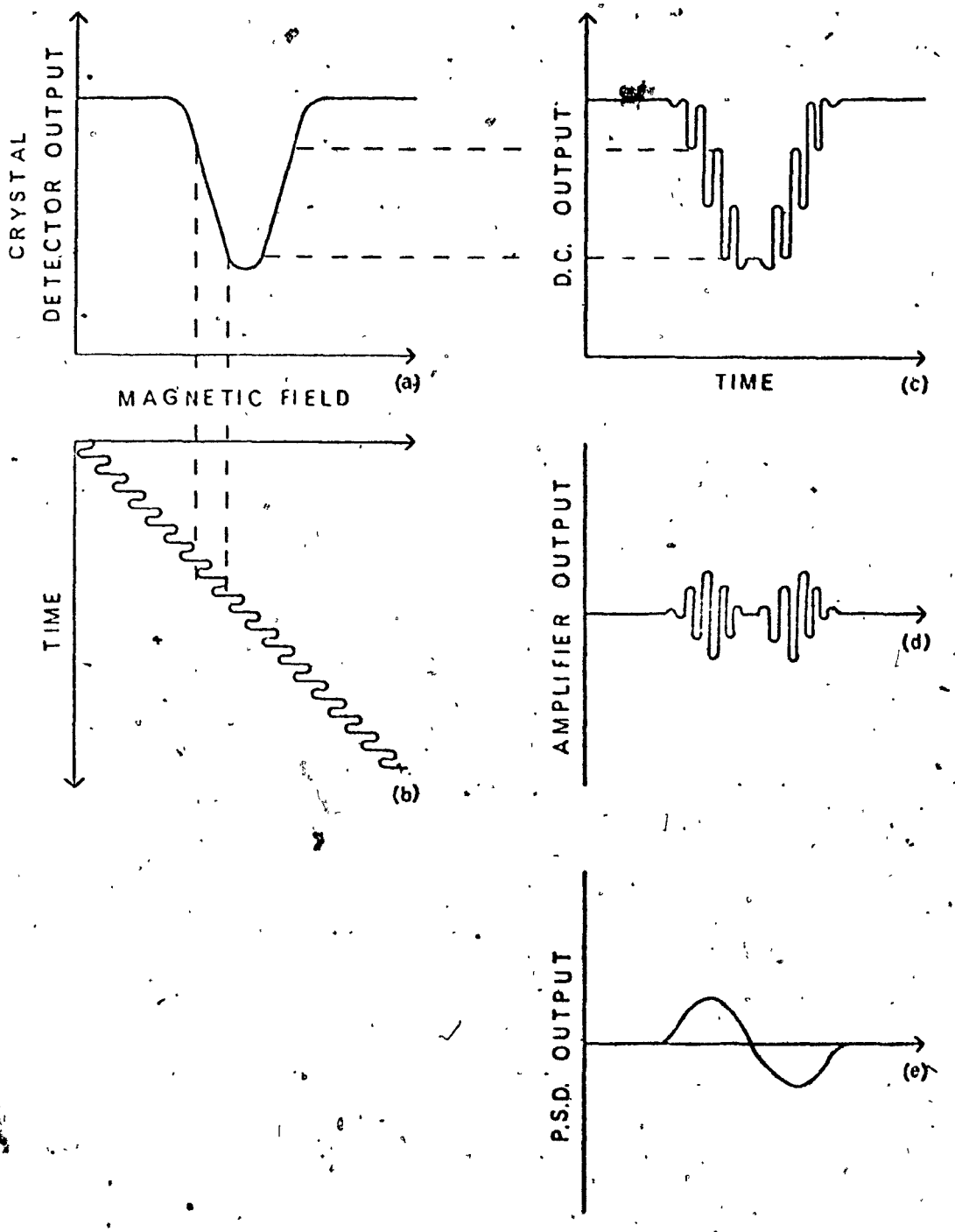

Fig. 3 Waveforms illustrating the operation of a spectrometer

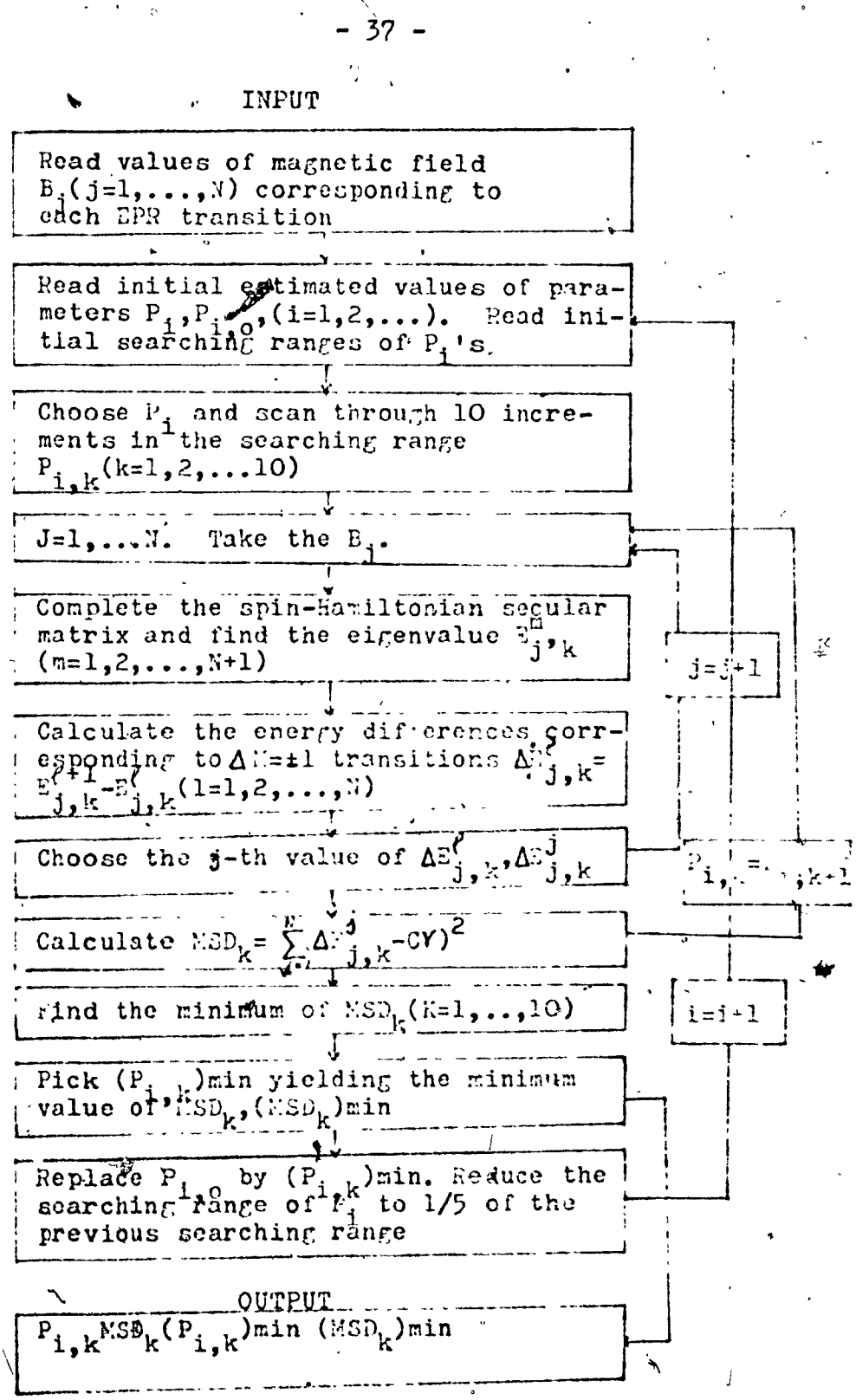

Fig. 4. Block diagram illustrating the computational procedure for determining the best-fit spin-Hamiltonian parameters

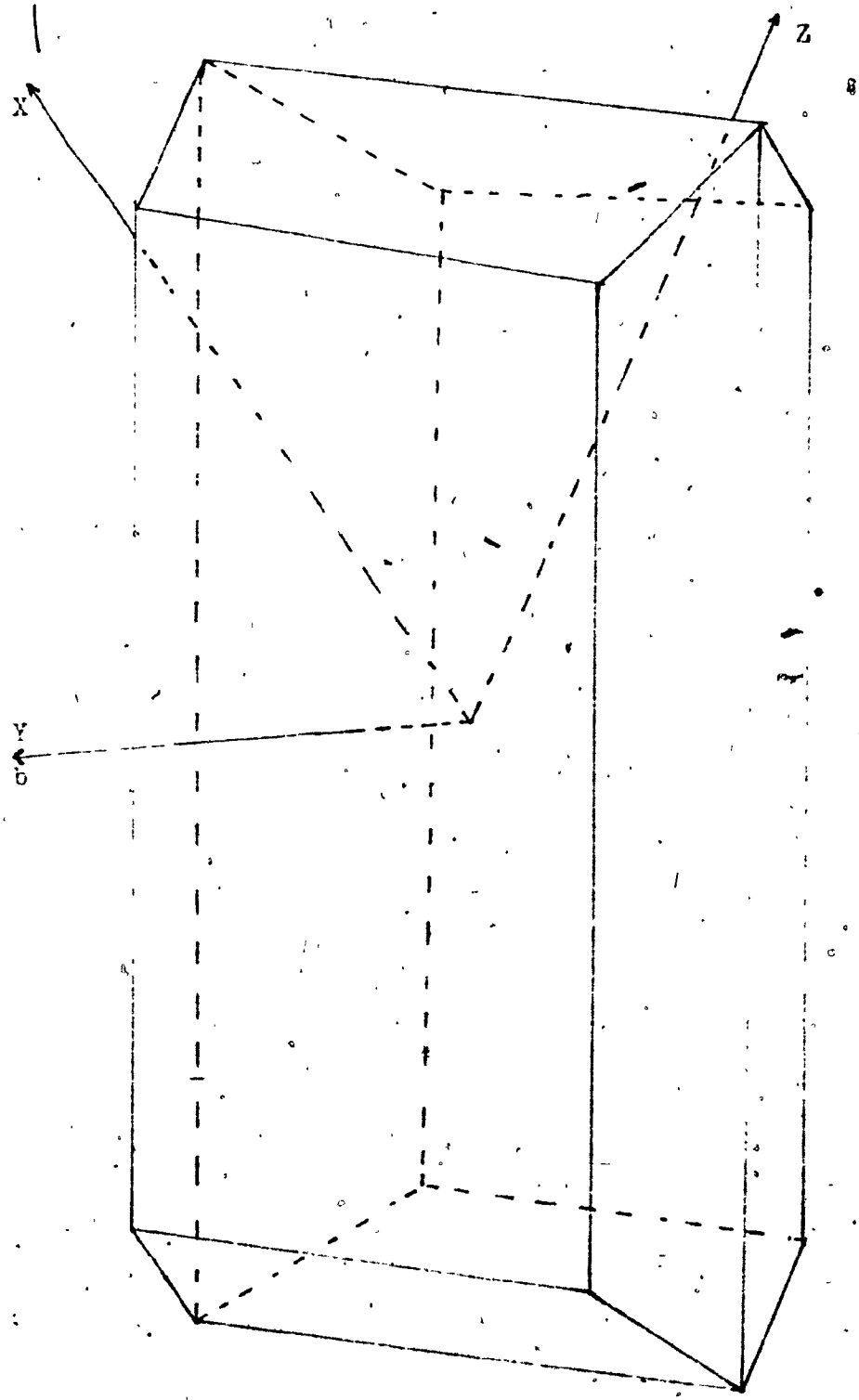

Figure 5. Monoclinic crystal for the $NdCl_3.6H_2O$, $SmCl_3.6H_2O$, $YCl_3.6H_2O$

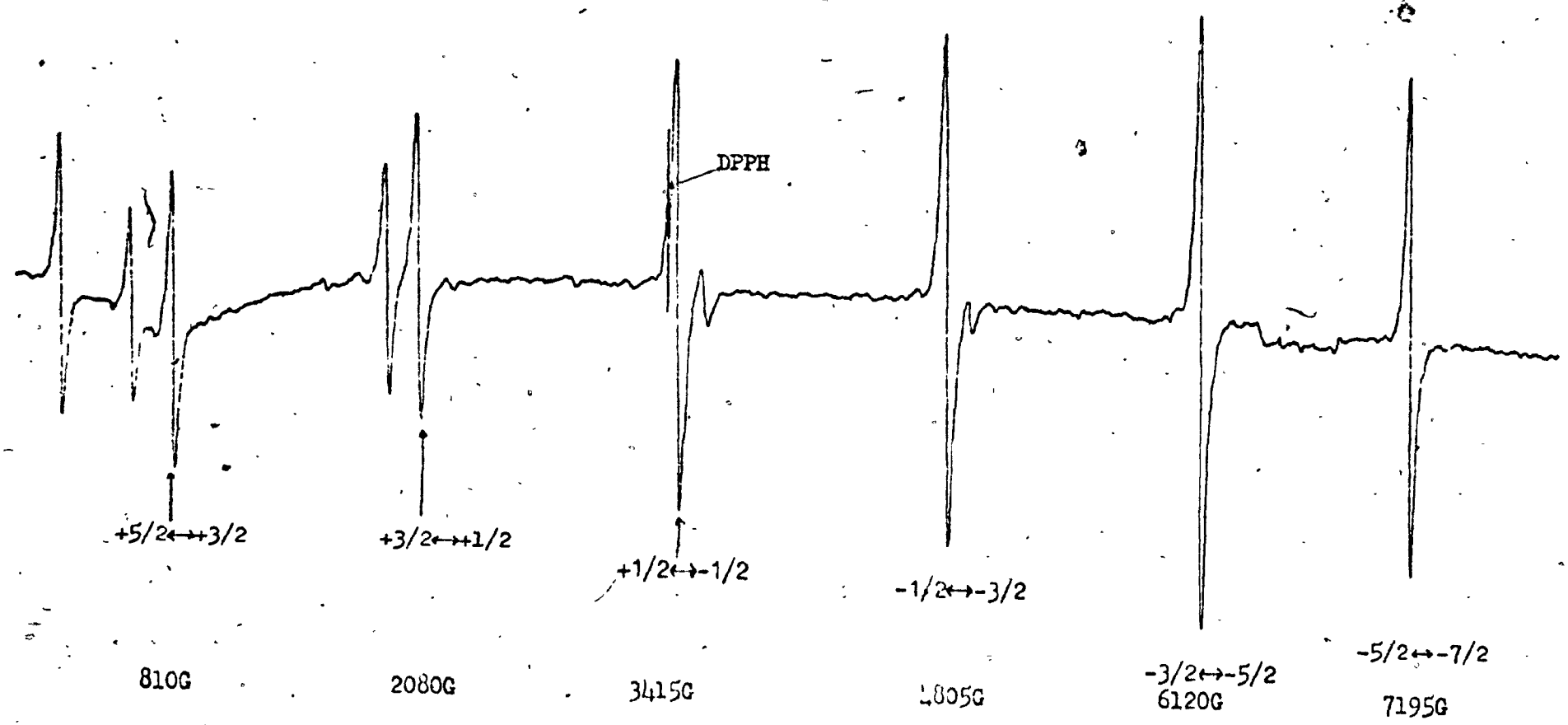

FIGURE 6 EPR SPECTRUM OF Gd^{3+} in a single crys[redacted]$\cdot 6H_2O$ ($\theta=0°$)

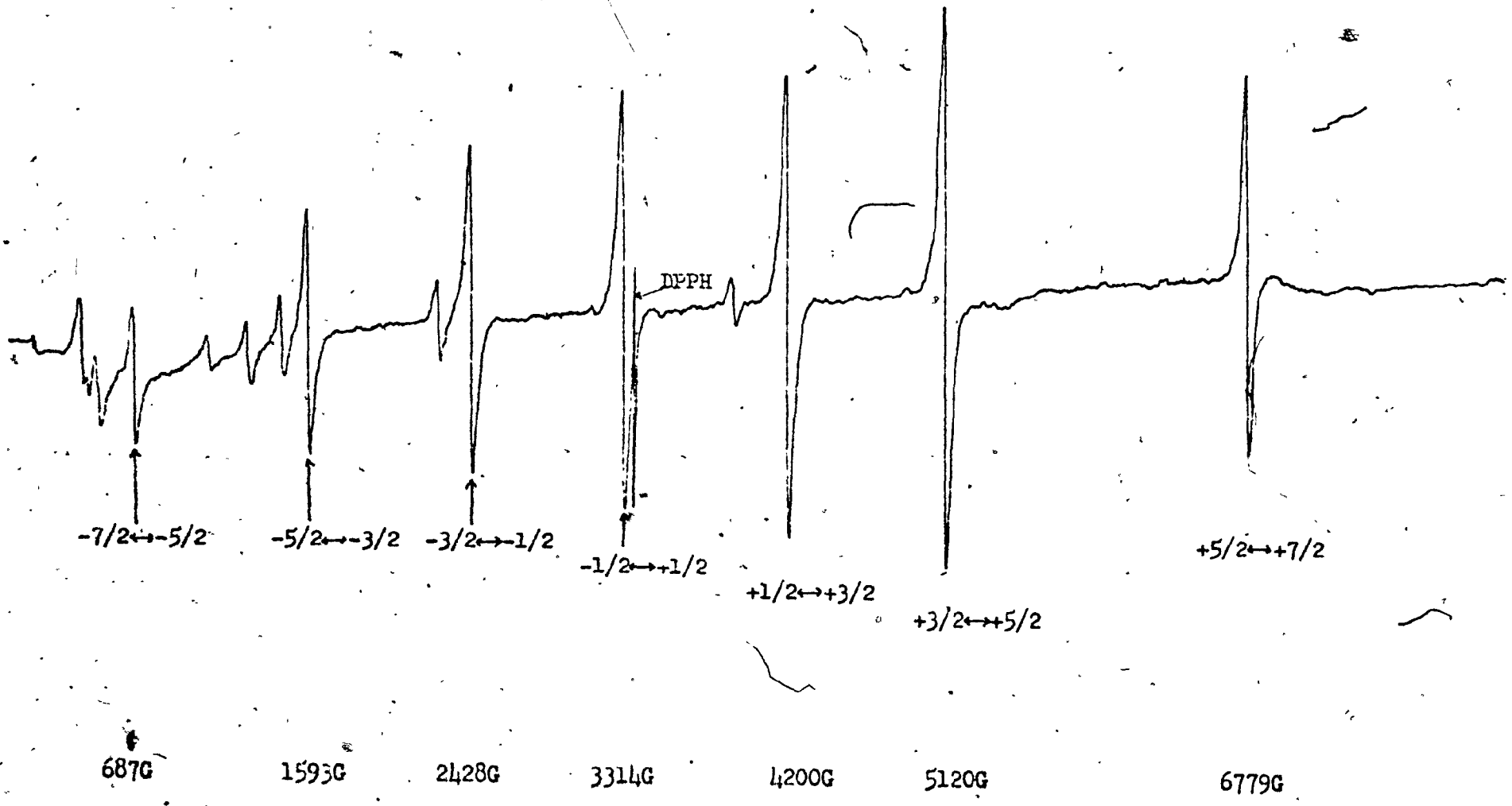

FIGURE 7. EPR SPECTRUM OF Gd^{3+} in a single crystal of $NdCl_3.6H_2O$ ($\theta=90^{\circ}$)

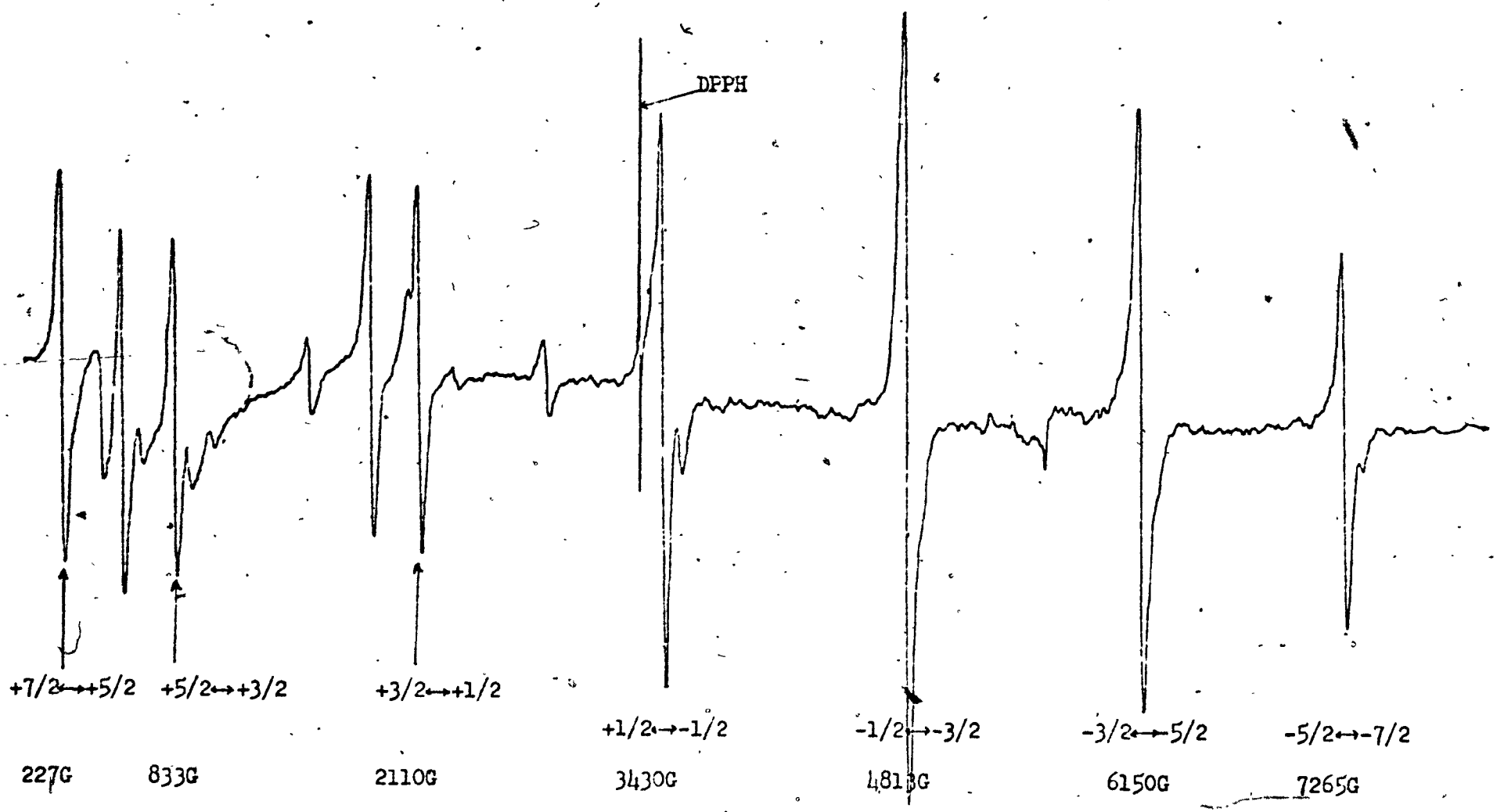

FIGURE 8 EPR SPECTRUM OF Gd^{3+} in a single crystal of $YCl_3.6H_2O$ ($\theta=0^\circ$)

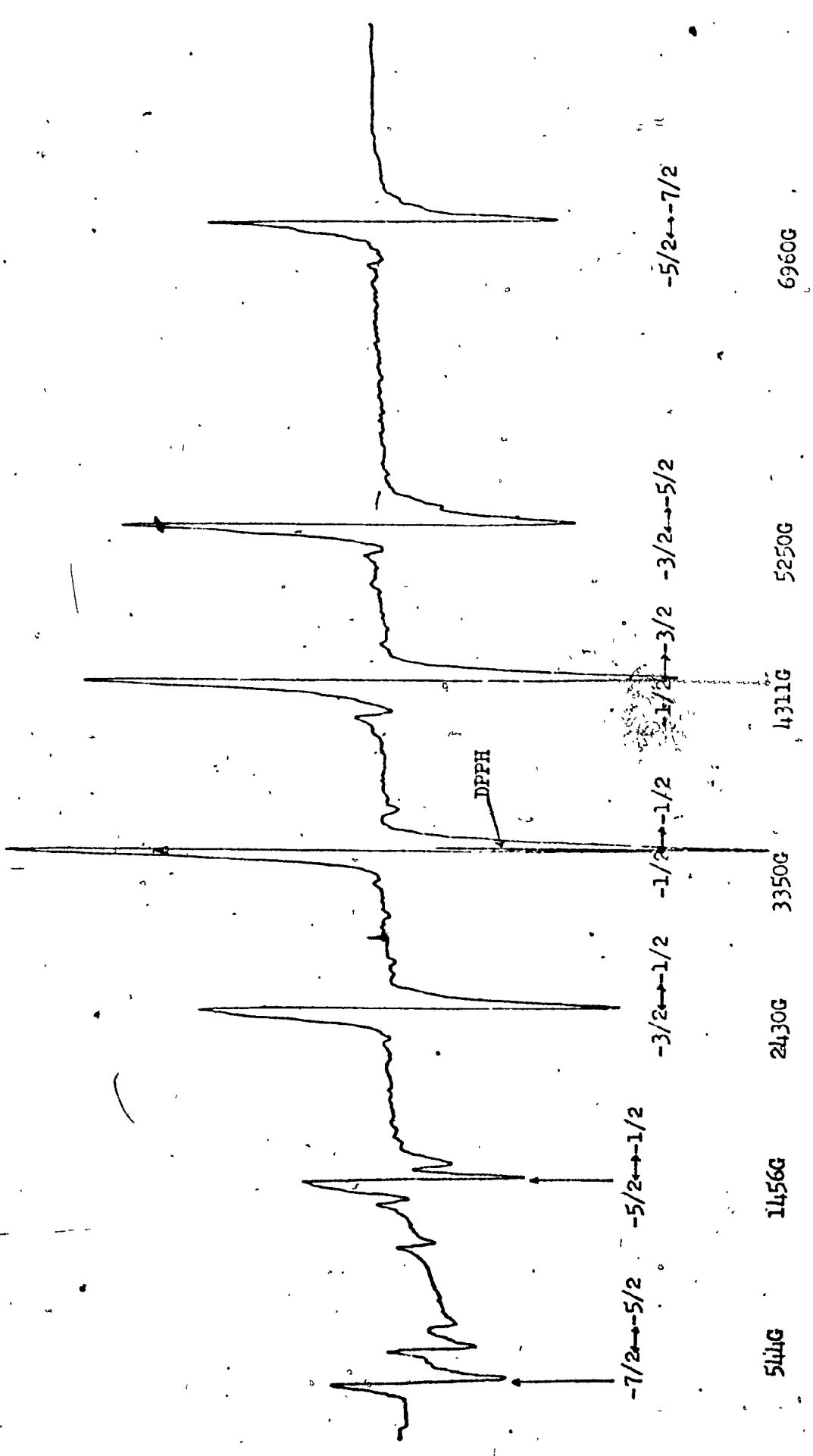

FIGURE 9. EPR SPECTRUM OF Gd^{3+} in a single crystal of $YCl_3.6H_2$) (θ=90°)

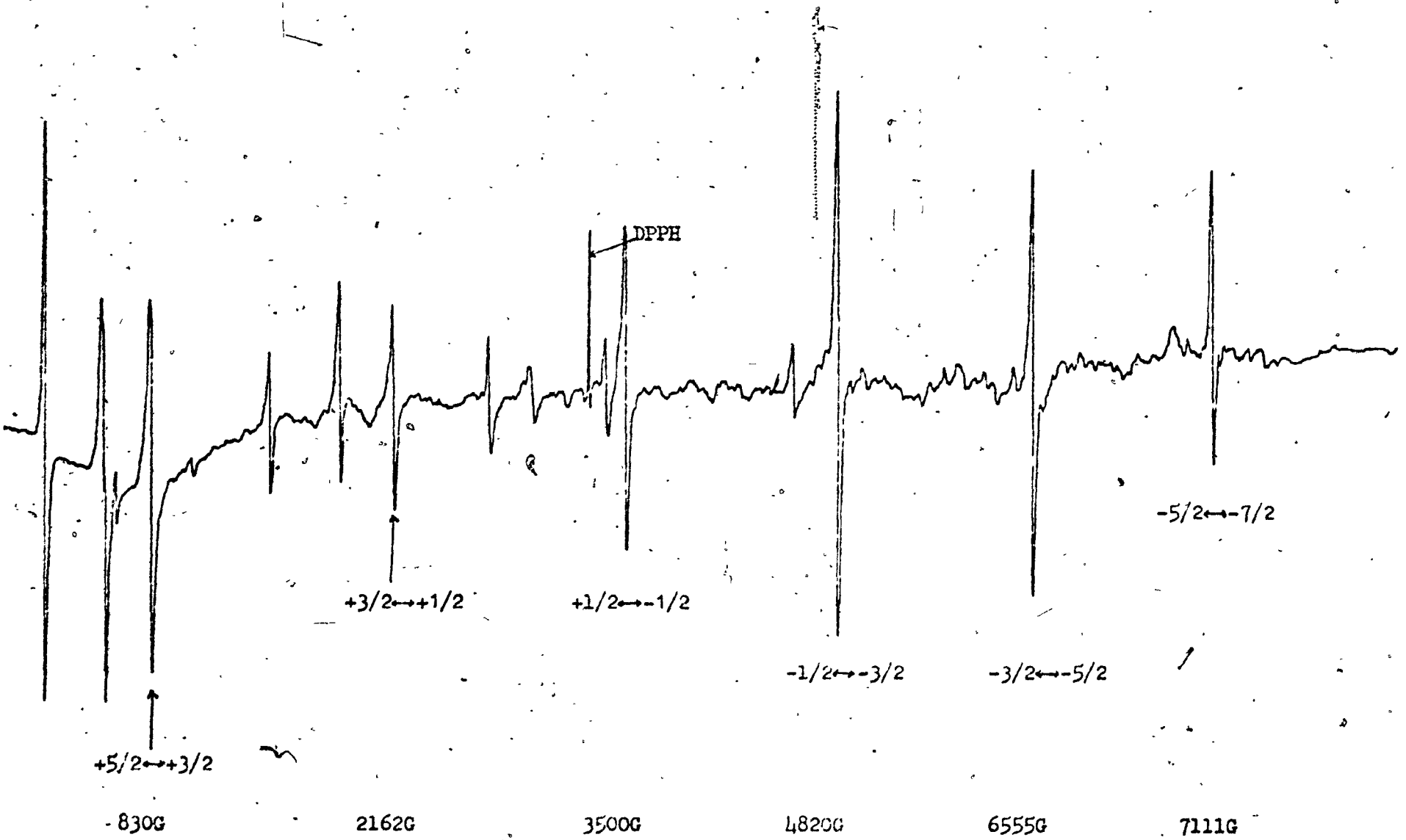

FIGURE 10. EPR SPECTRUM OF Gd^{3+} in single crystal of $SmCl_3.6H_2O$ ($\theta=0^\circ$)

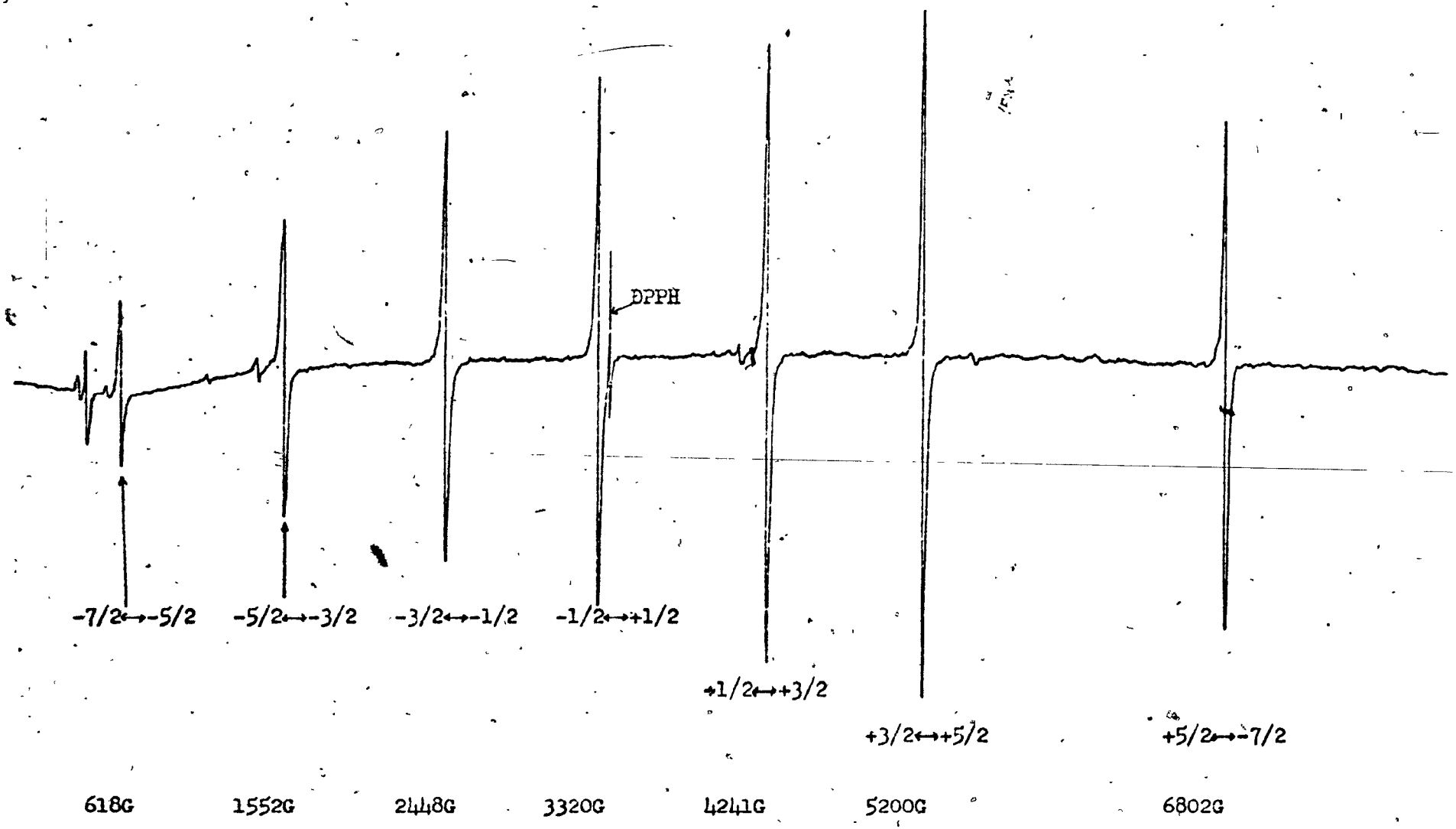

FIGURE 11 . EPR SPECTRUM OF Gd^{3+} in a single crystal of $SmCl_3.6H_2O$ ($\theta=90^\circ$)

TABLE I

ANGULAR VARIATION OF THE $\Delta M=\pm 1$ EPR TRANSITIONS OF Gd^{3+} IN $SmCl_3.6H_2O$

	-7/2↔-5/2	-5/2↔-3/2	-3/2↔-1/2	-1/2↔1/2	1/2↔3/2	3/2↔5/2	5/2↔7/2
0°	7111	6055	4820	3500	2162	830	
2°	7075	6065	4821	3502		830	
4°	7000	6056		3504			
6°			4870		2162		
8°	6610	6025		3544			
10°			4965				
12°	5927	5910		3615	2162	831	
14°			5022				
16°	5257	5700	5065		2242	832	
18°			5079	3805			
20°	3710	5317				838	
22°			5062		2398		
24°	2310	4752		4092			
26°			4980			860	
28°	1748				2560		
30°		3860	4830	4324			
32°	1430					910	
34°					2793		
36°	1210	3100	4480	4518			
38°						1060	
40°	1070			4576	3358		
42°		2580	3996				
44°	950			4570			
46°						1310	
48°	870		3500	4500	4150		
50°							
52°	810	2078					
54°			3180	4286			
56°	760	1950			4577	1880	
58°							
60°	720		2930	4000		3150	
62°					4750		
64°					4758	4110	
66°	670			3710	4750		
68°			2698				
70°		1710			4653	4984	
72°				3530			1678
74°			2590				2560
76°	630				4450	5410	3250
78°				3425			
80°		1592	2500		4304	5900	4965
82°						5498	
84°				3355	4240	5432	6104
86°							
88°					4236	5277	6680
90°	618	1552	2448	3320	4241	5200	6802

The values in the above table are in units of gauss.

TABLE II

ANGULAR VARIATION OF THE $\Delta M=\pm 1$ EPR TRANSITIONS OF Gd^{3+} IN $NdCl_3.6H_2O$

	-7/2↔-5/2	-5/2↔-3/2	-3/2↔-1/2	-1/2↔1/2	1/2↔3/2	3/2↔5/2	5/2↔7/2
0°	7195	6120	4805	3415	2080	810	
2°				3425	2085	810	
4°	7100	6035	4830				
6°				3470	2090	810	
8°	6740	5930	4920				
10°				3560	2120	818	
12°							
14°	5580	5720	5000				
16°				3760	2200	830	
18°	4080	5420	5020				
20°							
22°	2385	5040	4960	4020	2360	845	
24°							
26°	1700	4600	4870				
28°				4280	2615	880	
30°							
32°	1300	3660	4620				
34°				4415	3080	960	
36°	1160	3190	4370				
38°				4480	3425	1065	
40°							
42°	995	2620	3980	4460	3760	1185	
44°							
46°				4413	4060	1300	
48°	840	2260	2560				
50°				4280	4280	1505	
52°							
54°	800	2030	3200	4120	4460	2090	
56°							
58°				3940	4525	3290	
60°	770	1880	2960				
62°				3800	4570	4180	802
64°							
66°	730	1780	2740	3665	4500	4620	1700
68°							
70°				3580	4440	5040	2980
72°	694	1670	2590				
74°				3465	4320	5280	4080
76°							
78°	690	1620	2500	3400	4260	5345	5185
80°							
82°				3360	4220	5280	6170
84°	690	1610	2460				
86°				3320	4210	5150	6750
88°							6779
90°	687	1593	2428	3314	4200	5120	6779

The values in the above table are in units of gauss.

TABLE III

ANGULAR VARIATION OF THE $\Delta M=\pm 1$ EPR TRANSITIONS OF Gd^{3+} IN $YCl_3.6H_2O$

	-7/2↔-5/2	-5/2↔-3/2	-3/2↔-1/2	-1/2↔1/2	1/2↔3/2	3/2↔5/2	5/2↔7/2
0°	7265	6150	4813	3430	2110	833	227
2°	7200	6170					
4°	7105	6169	4875	3460			227
6°	6900	6147					
8°	6650	6125	4965	3510	2116	840	
10°	6280						
12°	5780	5920	5040	3660			
14°					2200		
16°		5660					
18°		5540	5140	3880	2280	850	230
20°			5120				
22°		4850	5100	4080			
24°					2465		
26°							
28°		3985	4900	4395	2610	890	258
30°							
32°		3270	4680	4520			
34°					2970	980	
36°							
38°	850	2640	4270	4640	3390	1090	310
40°				4641			
42°		2320	3815				
44°	680			4640	3910	1250	
46°							
48°		2055	3390	4530	4290	1460	375
50°							
52°		1940	3140				
54°				4310	4640	1685	
56°							
58°		1760	2910	4105	4800	2110	520
60°							
62°		1670	2785		4845	4310	
64°	580				4840		
66°							
68°		1590	2610	3640	4760	5040	660
70°							
72°		1545	2520			5380	770
74°	560			3510	4570		
76°							
78°		1490	2460	3431	4400	5620	980
80°						5616	5740
82°		1468					6418
84°	550		2432	3390	4316	5540	6680
86°							
88°		1459		3370		5320	6940
90°	544	1456	2430	3350	4311	5250	6960

The values in the above table are in units of gauss.

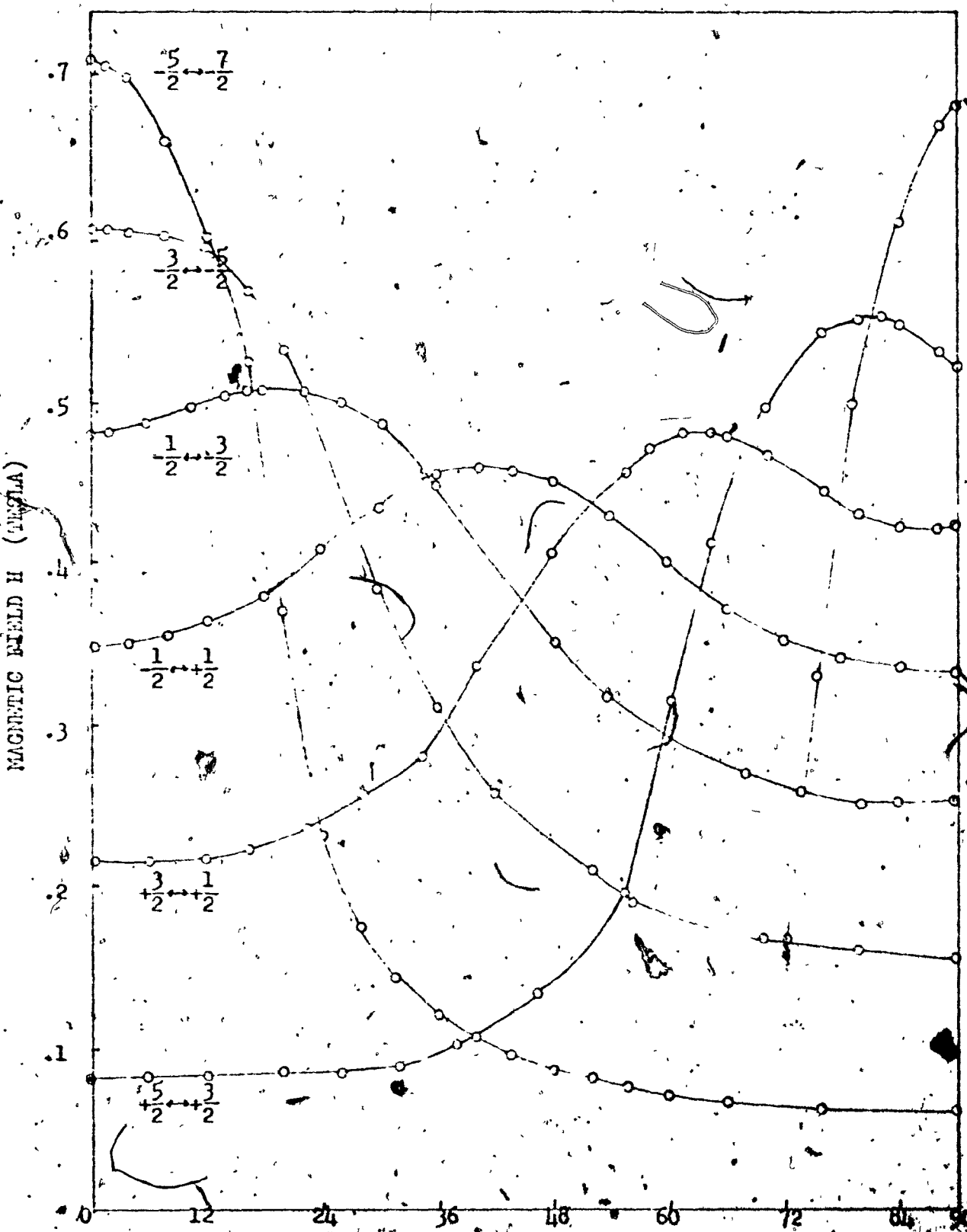

FIGURE 12 Angular variation of the EPR spectrum of Gd^{3+} in $SmCl_3.6H_2O$ single crystal (ν=9.443256 2GHz)
Data taken from Table I.

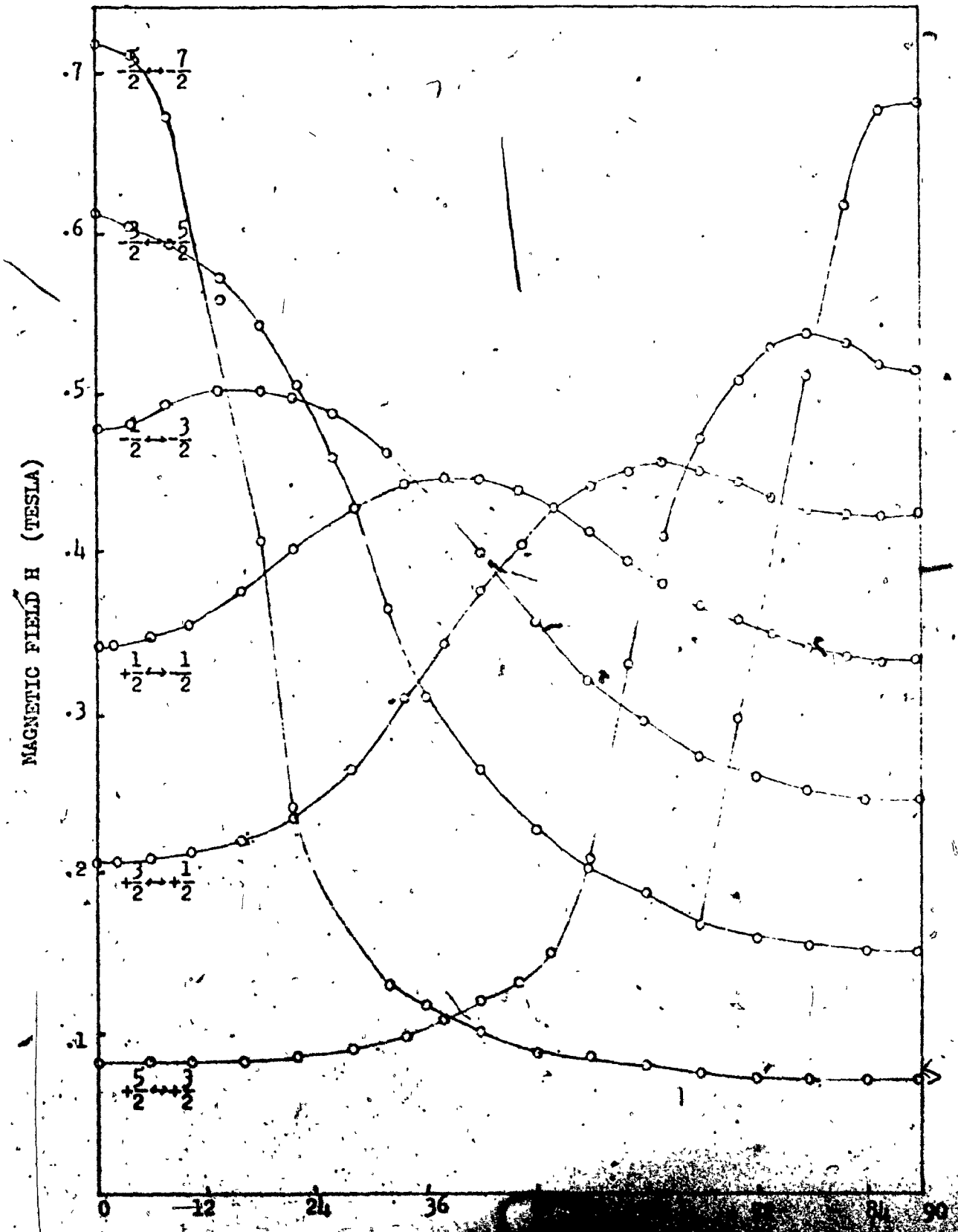

FIGURE 13 Angular variation [illegible] crystal [illegible]

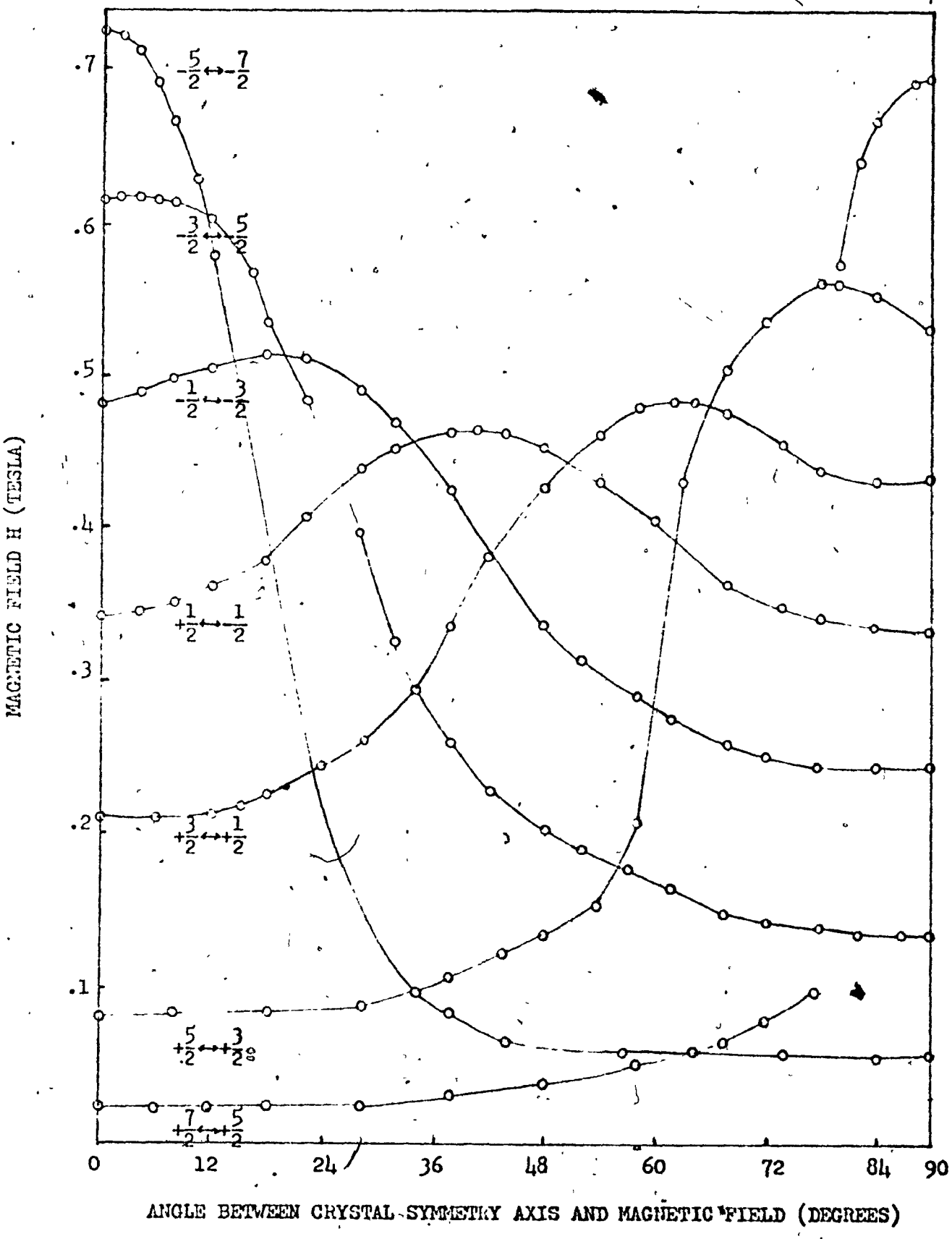

FIGURE 14 Angular variation of the EPR spectrum of Gd^{3+} in $YCl_3.6H_2O$ single crystal (ν=9.4506888GHz).
Data taken from Table III

APPENDIX I

The Secular Determinant of the Spin-Hamiltonian

	7/2	5/2	3/2	1/2	-1/2	-3/2	-5/2	-7/2
7/2	$3.5\sigma\beta H + 7b_2^0 + 7b_4^0 + b_6^0$	0	$\sqrt{7/3}b_2^2 + \sqrt{4/2}b_4^2 + 2/\sqrt{21}b_6^2$	0	$\sqrt{7/5}b_4^4 + \sqrt{5/7}b_6^4$	0	$2/\sqrt{7}b_6^6$	0
5/2	0	$2.5\sigma\beta H + b_2^0 - 13b_4^0 - 9b_6^0$	0	$\sqrt{5}b_2^2 + 1/\sqrt{20}b_4^2 - 2/\sqrt{5}b_6^2$	0	$\sqrt{5}b_4^4 - 1/\sqrt{5}b_6^4$	0	$2/\sqrt{7}b_6^6$
3/2	$\langle 7/2 \| 3/2 \rangle$	0	$1.5\sigma\beta H - 3b_2^0 - 3b_4^0 + 9b_6^0$	0	$2\sqrt{5/3}b_2^2 - 2\sqrt{3/2}b_4^2 + 4\sqrt{3/5}b_6^2$	0	$\langle 5/2 \| -3/2 \rangle$	0
1/2	0	$\langle 5/2 \| 1/2 \rangle$	0	$\sigma\beta H - 9b_2^0 + 9b_4^0 - b_6^0$	0	$\langle 3/2 \| -1/2 \rangle$	0	$\langle 1/2 \| -1/2 \rangle$
-1/2	$\langle 7/2 \| -1/2 \rangle$	0	$\langle 5/2 \| -1/2 \rangle$	0	$-\sigma\beta H - 9b_2^0 + 9b_4^0 - b_6^0$	0	$\langle 3/2 \| 1/2 \rangle$	0
-3/2	0	$\langle 5/2 \| -3/2 \rangle$	0	$\langle 3/2 \| -1/2 \rangle$	0	$-1.5\sigma\beta H - 3b_2^0 - 3b_4^0 + 9b_6^0$	0	$\langle 1/2 \| 3/2 \rangle$
-5/2	$\langle 7/2 \| 1/2 \rangle$	0	$\langle 5/2 \| -3/2 \rangle$	0	$\langle 3/2 \| 1/2 \rangle$	0	$-2.5\sigma\beta H + b_2^0 - 13b_4^0 - 9b_6^0$	0
-7/2	0	$\langle 7/2 \| -5/2 \rangle$	0	$\langle 5/2 \| -1/2 \rangle$	0	$\langle 7/2 \| 3/2 \rangle$	0	$-3.5\sigma\beta H + 7b_2^0 + 7b_4^0 + b_6^0$

APPENDIX II

COMPUTER PROGRAM USED FOR THE CALCULATIONS

```
      DIMENSION B(7),P(11,10),DP(11),E(7,10,3),TE(7,10,7),TTE(7,10),
     1SMD(10),S(5,5),R(9,1)
      BP=13.936
C     THE FOLLOWING ARE VALUES OF PARAMETERS FOR NDCL3.6H2O
      DATA(B(J),J=1,6)/.0[illegible]3,.20[illegible],.348199,.4[illegible],.612022,.719449/
      HN=9.4[illegible]3
      P(1,1)=1.95749
      P(2,1)=1.824
      P(3,1)=-1.183
      P(4,1)=.0963
      P(5,1)=-.0317
      P(6,1)=-.0254
      P(7,1)=-.0082
      P(8,1)=.023
      P(9,1)=-.00415
      P(10,1)=-.00055
C     THE FOLLOWING ARE INCREMENTS FOR ALL THE HOSTS
      DP(1)=.01
      DP(2)=.01
      DP(3)=.01
      DP(4)=.001
      DP(5)=.001
      DP(6)=.001
      DP(7)=.001
      DP(8)=.001
      DP(9)=.0001
      DP(10)=.0001
C     THE FOLLOWING ARE VALUES OF PARAMETERS FOR YCL3.6H2O
      DATA(B(J),J=1,6)/.0[illegible],.210[illegible],.3831,.4[illegible]1[illegible],.61[illegible],.7265/
      HN=9.4[illegible]
      P(1,1)=1.9[illegible]4
      P(2,1)=1.8134
      P(3,1)=-1.1[illegible]66
      P(4,1)=.09824
      P(5,1)-.03176
      P(5,1)=-P(5,1)
      P(6,1)=-.02546
      P(7,1)=- .00[illegible]26
      P(8,1)= .02294
      P(9,1)=-.00416
      P(10,1)=-.00056
C     THE FOLLOWING ARE VALUES OF PARAMETERS FOR SMCL3.6H2O
      DATA(B(J),J=1,6)/.0[illegible],.2160,.3500,.4813,.6[illegible]5,.7111/
      HN=9.401471621
      P(1,1)=1.991
      P(2,1)=1.8241
      P(3,1)=-1.188
      P(4,1)=.0983
      P(5,1)=-.0317
      P(6,1)=-.0254
      P(7,1)=-.0082
      P(8,1)=.023
      P(9,1)=-.00415
      P(10,1)=-.00055
C     THE ABOVE WERE PARAM., MAG. FIELD,AND FREQ. FOR THE VARIOUS CASES
      R3=SQRT(3.0)
      R5=SQRT(5.0)
      R7=SQRT(7.0)
   10 DO 55 I=1,10
```

```
      DO 80 K=1,10
      DO 70 J=1,6
      DO 7 IM=1,10
      IF(IM-I)6,5,6
    5 P(I,K)=P(I,1)+(K-1)*DP(I)
      GO TO 7
    6 P(IM,K)=P(IM,1)
    7 CONTINUE
      DO 100 IA=1,8
      DO 100 JA=1,8
      S(IA,JA)=0.0
  100 R(IA,JA)=0.0
      PBB=P(1,K)*BG*B(J)
      S(1,1)=3.5*PBB+7.*P(2,K)+7.*P(5,K)+P(10,K)
      S(2,2)=2.5*PBB+P(2,K)-13.*P(5,K)-5.*P(10,K)
      S(3,3)=1.5*PBB-3.*P(2,K)-3.*P(5,K)+3.*P(10,K)
      S(4,4)=.5*PBB-5.*P(2,K)+9.*P(5,K)-5.*P(10,K)
      S(5,5)=S(4,4)-PBB
      S(6,6)=S(3,3)-3.*PBB
      S(7,7)=S(2,2)-5.*PBB
      S(8,8)=S(1,1)-7.*PBB
      S(1,3)=R7*P(3,K)/R3+R7*R3*P(6,K)/2.+2.*P(7,K)/(R7*R3)
      S(1,5)=R7*P(4,K)/R5+R5*P(8,K)/R7
      S(1,7)=2.*P(9,K)/R7
      S(2,4)=R5*P(3,K)+P(6,K)/(R5*2.)-P(7,K)*2./R5
      S(2,6)=R3*P(4,K)-P(8,K)/R3
      S(3,5)=2.*R5*P(3,K)/R3-2.*P(6,K)*R3/R5+4.*R3*P(7,K)/R3
      S(2,6)=S(1,7)
      S(3,1)=S(1,3)
      S(3,7)=S(2,6)
      S(4,2)=S(2,4)
      S(4,6)=S(3,5)
      S(4,8)=S(1,5)
      S(5,1)=S(1,5)
      S(5,3)=S(3,5)
      S(5,7)=S(2,4)
      S(6,2)=S(2,6)
      S(6,4)=S(3,5)
      S(6,8)=S(1,3)
      S(7,1)=S(1,7)
      S(7,3)=S(2,6)
      S(7,5)=S(2,4)
      S(8,2)=S(1,7)
      S(8,4)=S(1,5)
      S(8,6)=S(1,3)
      CALL JACOBI (8,S,1,AR,R)
      DO 50 M=1,8
      E(J,K,M)=S(M,M)
   50 CONTINUE
      DO 60 L=1,7
      L1=L+1
      TE(J,K,L)=ABS(E(J,R,L1)-E(J,K,L))
   60 CONTINUE
      JJ=J+1
      TTE(J,K)=TE(J,K,JJ)
   70 CONTINUE
      SMD(K)=0.0
      DO 71 J=1,6
      SMD(K)=SMD(K)+(TTE(J,K)-HN)**2
   71 CONTINUE
```

```
 87 FORMAT(F15.8)
 80 CONTINUE
    SSMD=SMD(1)
    DO 82 K=1,10
    IF(SMD(K)-SSMD) 81,82,82
 81 SSMD=SMD(K)
    P(I,1)=P(I,(K-1))
 82 CONTINUE
    DP(I)=DP(I)/5.
    WRITE (6,84)(P(II,1),II=1,10)
 84 FORMAT(6F10.5/5F10.5)
 85 CONTINUE
    WRITE(6,87) SSMD
    IF(SSMD-.0001) 110,110,101
101 DO 95 I=1,10
    DP(I)=DP(I)/2.
 95 CONTINUE
    GO TO 10
110 STOP
    END
```

```
      SUBROUTINE JACOBI (N,G,JVEC,M,V)
C     SUBPROGRAM FOR DIAGONALIZATION OF MATRIX G BY SUCCESSIVE ROTATIONS
      DIMENSION G(8,8),V(8,8),X(8),IH(8)
C
C     NEXT 8 STATEMENTS FOR SETTING INITIAL VALUES OF MATRIX V
C
      IF (JVEC) 10,15,10
   10 DO 14 I=1,N
      DO 14 J=1,N
      IF(I-J) 12,11,12
   11 V(I,J)=1.0
      GO TO 14
   12 V(I,J)=0.
   14 CONTINUE
C
   15 M=0
C     NEXT 6 STATEMENTS SCAN FOR LARGEST OFF DIAG. ELEM. IN EACH ROW
C     X(I) CONTAINS LARGEST ELEMENT IN IHT ROW
C     IH(I) HOLDS SECOND SUBSCRIPT DEFINING POSITION OF ELEMENT
C
      MI=N-1
      DO 30 I=1,MI
      X(I)=0.
      MJ=I+1
      DO 30 J=MJ,N
      IF (X(I)-ABS (G(I,J))) 20,20,30
   20 X(I)=ABS (G(I,J))
      IH(I)=J
   30 CONTINUE
C
C     NEXT 7 STATEMENTS FIND FOR MAXIMUM OF X(I)S FOR PIVOT ELEMENT
   40 DO 70 I=1,MI
      IF(I-1) 60,60,45
   45 IF (XMAX-X(I)) 60,70,70
   60 XMAX=X(I)
      IP=I
      JP=IH(I)
   70 CONTINUE
C
C     NEXT 2 STATEMENTS TEST FOR XMAX, IF LESS THAN 10**-8,GO TO 1000
C
      EPSI=1.E-8
      IF(XMAX-EPSI) 1000,1000,148
C
  148 M=M+1
C
C     NEXT 11 STATEMENTS FOR COMPUTING TANG,SINE,COSN,G(I,I),G(J,J)
C
      IF (G(IP,IP)-G(JP,JP)) 150,151,151
  150 TANG=-2.*G(IP,JP)/(ABS(G(IP,IP)-G(JP,JP))+SQRT((G(IP,IP)-G(JP,JP)
     1)**2+4.*G(IP,JP)**2))
      GO TO 160
  151 TANG=+2.*G(IP,JP)/(ABS(G(IP,IP)-G(JP,JP))+SQRT((G(IP,IP)-G(JP,JP)
     1)**2+4.*G(IP,JP)**2))
  160 COSN=1.0/SQRT(1.0+TANG**2)
      SINE=TANG*COSN
      GII=G(IP,IP)
      G(IP,IP)=COSN**2*(GII+TANG*(2.*G(IP,JP)+TANG*G(JP,JP)))
      G(JP,JP)=COSN**2*(G(JP,JP)-TANG*(2.*G(IP,JP)-TANG*GII))
```

```
C
      G(IP,JP)=0.
C
C       NEXT 4 STATEMENTS FOR PSEUDO RANK OF THE EIGENVALUES
      IF (G(IP,IP)-G(JP,JP)) 152,153,153
  152 TEMP=G(IP,IP)
      G(IP,IP)=G(JP,JP)
      G(JP,JP)=TEMP
C
C     NEXT 6 STATEMENTS FOR ADJUSTING SIN,COS FOR COMPUTATATION OF G(I,K),V(I,
C
      IF(SINE) 154,155,155
  154 TEMP=+COSN
      GO TO 170
  155 TEMP=-COSN
  170 COSN=ABS(SINE)
      SINE=TEMP
C
C     DETERMINE WHETHER A NEW MAXIMUM VALUE SHOULD BE COMPUTED SINCE
C     THE PRESENT MAXIMUM IS IN THE I OR J ROW
C
  153 DO 350 I=1,MI
      IF (I-IP) 210,350,200
  200 IF (I-JP) 210,350,210
  210 IF (IH(I)-IP) 230,240,230
  230 IF (IH(I)-JP) 350,240,350
  240 K= IH(I)
      TEMP=G(I,K)
      G(I,K)=0.
      MJ=I+1
      X(I)=0.
C
C     NEXT 5 STATEMENTS SEARCH IN DEPLETED ROW FOR NEW MAXIMUM
C
      DO 320 J=MJ,N
      IF (X(I)-ABS(G(I,J))) 300,320,320
  300 X(I)=ABS(G(I,J))
      IH(I)=J
  320 CONTINUE
      G(I,K)=TEMP
  350 CONTINUE
C
      X(IP)=0.
      X(JP)=0.
C
C       NEXT 30 STATEMENTS FOR CHANGING THE OTHER ELEMENTS OF G
C
      DO 530 I=1,N
C
      IF (I-IP) 370,530,420
  370 TEMP=G(I,IP)
      G(I,IP)=COSN*TEMP+SINE*G(I,JP)
      IF (X(I)-ABS(G(I,IP))) 380,390,390
  380 X(I)=ABS(G(I,IP))
      IH(I)=IP
  390 G(I,JP)=-SINE*TEMP+COSN*G(I,JP)
      IF (X(I)-ABS(G(I,JP))) 400,530,530
  400 X(I)=ABS(G(I,JP))
      IH(I)=JP
      GO TO 530
```

```
C
  420 IF (I-JP) 430,530,480
  430 TEMP=Q(IP,I)
      Q(IP,I)=COSN*TEMP+SINE*Q(I,JP)
      IF (X(IP)-ABS(Q(IP,I))) 440,450,450
  440 X(IP)=ABS(Q(IP,I))
      IH(IP)=I
  450 Q(I,JP)=-SINE*TEMP+COSN*Q(I,JP)
      IF (X(I)-ABS(Q(I,JP))) 400,530,530
C
  480 TEMP=Q(IP,I)
      Q(IP,I)=COSN*TEMP+SINE*Q(JP,I)
      IF(X(IP)-ABS(Q(IP,I))) 490,500,500
  490 X(IP)=ABS(Q(IP,I))
      IH(IP)=I
  500 Q(JP,I)=-SINE*TEMP+COSN*Q(JP,I)
      IF (X(JP)-ABS(Q(JP,I))) 510,530,530
  510 X(JP)=ABS(Q(JP,I))
      IH(JP)=I
  530 CONTINUE
C
C     NEXT 6 STATEMENTS FOR TESTING COMPUTATION OF EIGENVECTORS
C
      IF (JVEC) 540,40,540
  540 DO 550 I=1,N
      TEMP=V(I,IP)
      V(I,IP)=COSN*TEMP+SINE*V(I,JP)
  550 V(I,JP)=-SINE*TEMP+COSN*V(I,JP)
      GO TO 40
 1000 RETURN
      END
```

BIBLIOGRAPHY

1. W. Low, Paramagnetic Resonance in Solids, Academic Press, New York (1960)
2. E. J. Zavoisky, J. Phys. (U.S.S.R.) 9.211 (1945)
3. H. A. Buckmaster and Y. H. Shing, Phys. Stat. Sol. (a) 12,325 (1972)
4.a H.E.D. Scovil, J. Feher and H. Seidel, Phys. Rev. 105,762 (1957)
4.b A. Abragam and B. Bleaney, Electron Paramagnetic Resonance of Transition Ions, Clarendon Press, Oxford (1970)
5. H. A. Buckmaster, R. Chatterjee and Y. H. Shing, Phys. Stat. Sol. (a) 13,9 (1972)
6. G. R.Sharp, Thesis, Sept. 1972, Sir George Williams University
7. H. A. Buckmaster, R. Chatterjee and Y. H. Shing, Magnetic Resonance 4,85-89 (1971)
8. G. B. Singh, G. C. Upreti and P. Venkateswarlu, J. Chem. Phys. 46,2885 (1967)
9. D. Meierling and W. Ullmann, Z. Naturf. 23a, 1971 (1968)
10. G. B. Singh and Putcha Venkateswarlu, Proc. Indian Acad. Sci. A. Vol. 65, No. 4,211 (1967)
11. R. Lacroix, Helv. Phys. Acta. 30,374 (1957)
12. B. G. Wybourne, Phys. Rev. 148,317 (1966)